Fumarate hydratase is a critical metabolic regulator of haematopoietic stem cell functions

Amelie V. Guitart[1,10], Theano I. Panagopoulou[1,10], Arnaud Villacreces[1], Milica Vukovic[1], Catarina Sepulveda[1], Lewis Allen[1], Roderick N. Carter[2], Louie N. van de Lagemaat[1,8], Marcos Morgan[1], Peter Giles[3], Zuzanna Sas[1], Marta Vila Gonzalez[1], Hannah Lawson[1], Jasmin Paris[1], Joy Edwards-Hicks[4], Katrin Schaak[1], Chithra Subramani[1], Deniz Gezer[1], Alejandro Armesilla-Diaz[1], Jimi Carlo Wills[4], Aaron Easterbrook[5], David Coman[6], Chi Wai Eric So[7], Donal O'Carroll[1], Douglas Vernimmen[8], Neil P. Rodrigues[9], Patrick J. Pollard[4,11], Nicholas M. Morton[2,11], Andrew Finch[4,11] & Kamil R. Kranc[1,4,*]

[1]MRC Centre for Regenerative Medicine, University of Edinburgh, Edinburgh, UK

[2]Centre for Cardiovascular Science, Queen's Medical Research Institute, University of Edinburgh, Edinburgh, UK

[3]Wales Gene Park & Wales Cancer Research Centre, Division of Cancer and Genetics, School of Medicine, Cardiff University, Cardiff, UK

[4]Edinburgh Cancer Research UK Centre, MRC Institute of Genetics and Molecular Medicine, University of Edinburgh, Edinburgh, UK

[5]Mater Children's Private Hospital Brisbane, Queensland, Australia

[6]Department of Metabolic Medicine, The Lady Cilento Children's Hospital, South Brisbane, Queensland, Australia

[7]Department of Haematological Medicine, Division of Cancer Studies, King's College London, London, UK

[8]The Roslin Institute, University of Edinburgh, UK

[9]The European Cancer Stem Cell Research Institute, School of Biosciences, Cardiff University, Cardiff, UK

[10]These authors contributed equally to this work, [11]These authors contributed equally to this work

[*]Corresponding author: kamil.kranc@ed.ac.uk

Running title: Fh1 is essential for HSC functions

Abbreviations used: AML, acute myeloid leukaemia; FL, foetal liver; Fh1, fumarate hydratase; HSCs, haematopoietic stem cells; LICs, leukaemia-initiating cells; OCR, oxygen consumption rate; TCA cycle, tricarboxylic acid cycle

Caption:

Guitart et al. performed an *in vivo* genetic dissection of the Krebs cycle enzyme fumarate hydratase (Fh1) in the haematopoietic system. Their investigations revealed multifaceted functions of Fh1 in the regulation of haematopoietic stem cell biology and leukemic transformation.

ABSTRACT

Strict regulation of stem cell metabolism is essential for tissue functions and tumour suppression. Here, we investigated the role of fumarate hydratase (Fh1), a key component of the mitochondrial tricarboxylic acid (TCA) cycle and cytosolic fumarate metabolism, in normal and leukaemic haematopoiesis. Haematopoiesis-specific *Fh1* deletion (resulting in endogenous fumarate accumulation and a genetic TCA cycle block reflected by decreased maximal mitochondrial respiration) caused lethal foetal liver haematopoietic defects and haematopoietic stem cell (HSC) failure. Re-expression of extra-mitochondrial *Fh1* (which normalised fumarate levels but not maximal mitochondrial respiration) rescued these phenotypes, indicating the causal role of cellular fumarate accumulation. However, HSCs lacking mitochondrial *Fh1* (which had normal fumarate levels but defective maximal mitochondrial respiration) failed to self-renew and displayed lymphoid differentiation defects. In contrast, leukaemia-initiating cells lacking mitochondrial *Fh1* efficiently propagated *Meis1/Hoxa9*-driven leukaemia. Thus we identify novel roles for fumarate metabolism in HSC maintenance and haematopoietic differentiation, and reveal a differential requirement for mitochondrial *Fh1* in normal haematopoiesis and leukaemia propagation.

INTRODUCTION

Successful clinical application of haematopoietic stem cells (HSCs) is critically dependent on their ability to give long-term multilineage haematopoietic reconstitution (Weissman and Shizuru, 2008). Multiple studies have revealed the paradigmatic transcription factors driving HSC self-renewal and differentiation to sustain multilineage haematopoiesis (Gottgens, 2015). Emerging evidence indicates that strict control of HSC metabolism is also essential for their life-long functions (Manesia et al., 2015; Suda et al., 2011), but the key metabolic regulators that ensure stem cell integrity remain elusive. Although highly proliferative foetal liver (FL) HSCs utilise oxygen dependent pathways for energy generation (Manesia et al., 2015; Suda et al., 2011), adult HSCs are known to suppress the flux of glycolytic metabolites into the mitochondrial TCA cycle and heavily rely on glycolysis to maintain their quiescent state (Simsek et al., 2010; Takubo et al., 2013; Wang et al., 2014). While pharmacological inhibition of glycolytic flux into the TCA cycle enhances HSC activity upon transplantation (Takubo et al., 2013), severe block of glycolysis (i.e. *Ldha* deletion) and a consequent elevated mitochondrial respiration abolishes HSC maintenance (Wang et al., 2014). The switch from glycolysis to mitochondrial oxidative metabolism is essential for adult HSC differentiation rather than maintenance of their self-renewing pool (Yu et al., 2013). Leukaemia-initiating cells (LICs) are even more dependent on glycolysis than normal HSCs (Wang et al., 2014). Partial or severe block in glycolysis (elicited by deletion of *Pkm2* or *Ldha*, respectively) and a metabolic shift to mitochondrial respiration efficiently suppress the development and maintenance of LICs (Lagadinou et al., 2013; Wang et al., 2014). Thus the maintenance of adult self-renewing HSCs and LICs appears to critically depend on glycolysis rather than the mitochondrial TCA, which is thought to be less important for this process. However, thus far, the requirement for any of the TCA enzymes in FL and adult HSC and LIC maintenance has not been investigated.

Genetic evidence in humans indicates that rare recessive mutations in the *FH* gene encoding a TCA enzyme fumarate hydratase result in severe developmental abnormalities, including haematopoietic defects (Bourgeron et al., 1994). Consistent with this, we also found that monozygous twins with

recessive *FH* mutations (Tregoning et al., 2013) display leukopenia and neutropenia (Table S1), thus suggesting a role for *FH* in the regulation of haematopoiesis. Mitochondrial and cytosolic fumarate hydratase enzyme isoforms, both encoded by the same gene (called *FH* in humans and *Fh1* in mice) (Sass et al., 2001; Stein et al., 1994), catalyse hydration of fumarate to malate. While mitochondrial Fh1 is an integral part of the TCA cycle, cytosolic Fh1 metabolises fumarate generated during arginine synthesis, the urea cycle, and the purine nucleotide cycle in the cytoplasm (Yang et al., 2013). Autosomal dominant mutations in *FH* are associated with hereditary leiomyomatosis and renal cell cancer indicating that *FH* functions as a tumour suppressor (Launonen et al., 2001; Tomlinson et al., 2002). Given that *FH* mutations have been associated with haematopoietic abnormalities and tumour formation, here we investigated the role of *Fh1* in normal and malignant haematopoiesis.

RESULTS

Fh1 is required for foetal liver haematopoiesis

Fh1 is uniformly expressed in mouse $Lin^-Sca\text{-}1^+c\text{-}Kit^+$ (LSK) $CD48^-CD150^+$ HSCs, $LSKCD48^-CD150^-$ multipotent progenitors (MPPs), primitive haematopoietic progenitor cells (i.e. $LSKCD48^+CD150^-$ HPC-1 and $LSKCD48^+CD150^+$ HPC-2 populations) and $Lin^-Sca\text{-}1^-c\text{-}Kit^+$ (LK) myeloid progenitors sorted both from FL (the major site of definitive haematopoiesis during development) of 14.5 dpc embryos and adult bone marrow (BM) (Fig. 1A). To determine the requirement for *Fh1* in HSC maintenance and multilineage haematopoiesis, we conditionally deleted *Fh1* specifically within the haematopoietic system shortly after the emergence of definitive HSCs using the *Vav-iCre* deleter strain (de Boer et al., 2003). We bred $Fh1^{fl/fl}$ mice (Pollard et al., 2007) with *Vav-iCre* mice and found no viable $Fh1^{fl/fl}$;*Vav-iCre* offspring (Table S2). $Fh1^{fl/fl}$;*Vav-iCre* embryos were recovered at 14.5 dpc at normal Mendelian ratios, suggesting foetal or perinatal lethality. FLs isolated from $Fh1^{fl/fl}$;*Vav-iCre* embryos appeared abnormally small and pale indicating severe impairment in FL haematopoiesis (Fig. 1B). *Fh1* loss from the haematopoietic system was confirmed by the absence of *Fh1* transcripts (Fig. 1C) in $CD45^+$ and $c\text{-}Kit^+$

haematopoietic cells from *Fh1*$^{fl/fl}$;*Vav-iCre* FLs and absence of Fh1 protein in FL c-Kit^{+} cells from *Fh1*$^{fl/fl}$;*Vav-iCre* embryos (Fig. 1D). While *Fh1*$^{fl/fl}$;*Vav-iCre* FLs had decreased numbers of haematopoietic cells due to reduced numbers of differentiated lineage^{+} (Lin^{+}) cells, the numbers of primitive FL Lin^{-} cells remained unchanged (Fig. 1E). Colony-forming cell (CFC) assays indicated the failure of *Fh1*-deficient FL cells to differentiate (Fig. 1F). Analyses of erythroid differentiation revealed a block of erythropoiesis resulting in severe anaemia (Fig. 1G). *Fh1* is therefore essential for multilineage differentiation of FL stem and/or progenitor cells.

***Fh1* is essential for HSC maintenance**

Next, we asked whether *Fh1* is required for the maintenance of the stem and progenitor cell compartments in FLs. FLs from *Fh1*$^{fl/fl}$;*Vav-iCre* embryos had normal absolute numbers of LK myeloid progenitors (Fig. 1H) and LSK stem and primitive progenitor cells (Fig. 1I) but displayed an increase in total numbers of HSCs compared to control FLs (Fig. 1J). To test the repopulation capacity of *Fh1*-deficient HSCs, we transplanted 100 CD45.2^{+} HSCs sorted from 14.5 dpc FLs into lethally irradiated syngeneic CD45.1^{+}/CD45.2^{+} recipients and found that *Fh1*-deficient HSCs failed to reconstitute short-term and long-term haematopoiesis (Fig. 1K-L). To test the possibility that *Fh1*-deficient FLs contain stem cell activity outside the immunophenotypically defined LSKCD48^{-}CD150^{+} HSC compartment, we transplanted unfractionated FL cells from *Fh1*$^{fl/fl}$;*Vav-iCre* and control embryos into lethally irradiated recipient mice (together with support BM cells) and found that *Fh1*-deficient FL cells failed to repopulate the recipients (Fig. 1M). Thus *Fh1* is dispensable for HSC survival and expansion in the FL but is critically required for HSC maintenance upon transplantation.

To establish the requirement for *Fh1* in adult HSC maintenance we generated *Fh1*$^{fl/fl}$;*Mx1-Cre* mice in which efficient recombination is induced by treatment with poly(I)-poly(C) (pIpC) (Kuhn et al., 1995). We mixed CD45.2^{+} BM cells from untreated *Fh1*$^{fl/fl}$;*Mx1-Cre*, *Fh1*$^{+/fl}$;*Mx1-Cre* or control mice with CD45.1^{+} BM cells, transplanted them into recipient mice and allowed for efficient

reconstitution (Fig. 1N). pIpC administration to the recipients of *Fh1*$^{fl/fl}$;*Mx1-Cre* BM cells resulted in a progressive decline of donor-derived CD45.2^{+} cell chimerism in PB (Fig. 1N) and a complete failure of *Fh1*-deficient cells to contribute to primitive and mature haematopoietic compartments of the recipients (Fig. 1O). Therefore, *Fh1* is critical for the maintenance of both FL and adult HSCs.

Fh1 deficiency results in cellular fumarate accumulation and decreased maximal mitochondrial respiration

We next investigated the biochemical consequences of *Fh1* deletion in primitive haematopoietic cells. To investigate how *Fh1* loss affects the oxidative phosphorylation capacity of primitive FL c-Kit^{+} haematopoietic cells, we measured oxygen consumption rate (OCR) under basal conditions and in response to sequential treatment with oligomycin (ATPase inhibitor), FCCP (mitochondrial uncoupler), and a concomitant treatment with rotenone and antimycin A (complex I and III inhibitors, respectively). The basal OCR was not affected in *Fh1*-deficient FL c-Kit^{+} cells, suggesting that the majority of mitochondrial NADH required for oxygen consumption in these cells originates from TCA-independent sources. However, the maximal OCR (after treatment with FCCP), which reflects maximal mitochondrial respiration, was profoundly decreased in *Fh1*-deficient cells (Fig. 2A) (but not in *Fh1*$^{+/fl}$;*Vav-iCre* cells; data not shown), indicating that *Fh1* deficiency may result in a compromised capacity to meet increased energy demands associated with metabolic stress or long-term survival (Choi et al., 2009; Ferrick et al., 2008; Keuper et al., 2014; van der Windt et al., 2012; Yadava and Nicholls, 2007). We also found that primitive *Fh1*-deficient FL haematopoietic cells failed to maintain ATP synthesis upon galactose-mediated inhibition of glycolysis (Fig. 2B, left panel), consistent with an increased reliance on glycolysis for ATP production. Furthermore, *Fh1*-deficient c-Kit^{+} cells had increased expression of glucose transporters (*Glut1* and *Glut3*) and key glycolytic enzymes *Hk2* and *Pfkp*, and displayed increased extracellular acidification rate (ECAR), indicative of enhanced glycolysis (Fig. 2C-D). Thus *Fh1* deficiency results in an increase in glycolytic flux and impaired maximal mitochondrial respiration.

To determine the impact of *Fh1* deletion on fumarate levels we performed mass spectrometry analyses. *Fh1*-deficient FL c-Kit$^+$ cells accumulated high levels of endogenous cellular fumarate (Fig. 2E), consistent with previous observations in non-haematopoietic tissues harbouring *Fh1* mutation (Adam et al., 2013). Under the conditions of elevated fumarate, argininosuccinate is generated from arginine and fumarate by the reversed activity of the urea cycle enzyme argininosuccinate lyase (Zheng et al., 2013). We found that argininosuccinate is produced at high levels in *Fh1*-deficient c-Kit$^+$ cells (Fig. 2F). Furthermore, fumarate, when accumulated at high levels, modifies cysteine residues in many proteins, forming S-(2-succinyl)-cysteine (2SC) (Adam et al., 2011; Alderson et al., 2006; Bardella et al., 2011; Ternette et al., 2013). *Fh1*-deficient c-Kit$^+$ cells exhibited high immunoreactivity for 2SC (Fig. 2G). Thus primitive haematopoietic cells lacking *Fh1* have compromised maximal mitochondrial respiration, display increased glycolysis, fail to maintain normal ATP production upon inhibition of glycolysis, and accumulate high levels of fumarate resulting in excessive protein succination.

Efficient fumarate metabolism is essential for HSC maintenance and multilineage haematopoiesis

Mechanistically, the phenotypes observed upon *Fh1* deletion could result from the genetic block in the TCA cycle or the accumulation of cellular fumarate (Adam et al., 2011; Pollard et al., 2007). To differentiate between these two mechanisms we employed mice ubiquitously expressing a human cytoplasmic isoform of FH (FH^{Cyt}, which lacks the mitochondrial targeting sequence and therefore is excluded from the mitochondria) (Adam et al., 2013). FH^{Cyt} does not restore defects in mitochondrial oxidative metabolism but normalises levels of total cellular fumarate (Adam et al., 2013; O'Flaherty et al., 2010). While primitive haematopoietic cells from FLs of *Fh1*$^{fl/fl}$;*FH*^{Cyt}*;Vav-iCre* embryos had normal mitochondrial membrane potential (data not shown) they displayed defective maximal respiration (Fig. 2A) and impaired compensatory mitochondrial ATP production upon inhibition of glycolysis (Fig. 2B, right panel), as well as an increase in ECAR (Fig. 2D) similar to *Fh1*$^{fl/fl}$;*Vav-iCre* FL cells. Furthermore, primitive *Fh1*$^{fl/fl}$;*FH*^{Cyt};*Vav-iCre* FL cells had

significantly reduced levels of cellular fumarate (Fig. 2E) and argininosuccinate (Fig. 2F), and undetectable immunoreactivity to 2SC (Fig. 2G), indicating that the biochemical consequences of fumarate accumulation were largely abolished by the *FH*^{Cyt} transgene expression. Although *FH*^{Cyt} transgene decreased overall cellular levels of fumarate, argininosuccinate and succinated proteins, we cannot exclude the possibility that fumarate is elevated in mitochondria and contributes to the impairment of mitochondrial function in the absence of mitochondrial Fh1. Collectively, while cells from *Fh1*$^{fl/fl}$;*FH*^{Cyt};*Vav-iCre* FL displayed impaired maximal respiration, they had cellular fumarate levels comparable to control cells.

Notably, *Fh1*$^{fl/fl}$;*FH*^{Cyt};*Vav-iCre* mice were born at normal Mendelian ratios (Table S3) and matured to adulthood without any obvious defects. BM cells from adult *Fh1*$^{fl/fl}$;*FH*^{Cyt};*Vav-iCre* mice efficiently generated myeloid colonies (Fig. 2H), had normal BM cellularity (Fig. 2I), and displayed multilineage haematopoiesis (Fig. 2J-K), despite reduced numbers of B cells (Fig. 2K). Furthermore, they had unaffected numbers of LK myeloid progenitor cells (Fig. 2L), and increased numbers of LSK cells (Fig. 2M) and HSCs (Fig. 2N). Therefore, it is critical that HSCs and/or primitive progenitor cells efficiently metabolise fumarate to sustain haematopoietic differentiation. Finally, HSCs that acquire mitochondrial Fh1 deficiency (which abolishes maximal mitochondrial respiration) shortly after their emergence manage to survive, expand in the FL, colonise the BM and sustain steady-state multilineage haematopoiesis, implying that mitochondrial Fh1 is largely dispensable for these processes.

Mitochondrial Fh1 deficiency compromises HSC self-renewal

To stringently test the long-term self-renewal capacity of HSCs lacking mitochondrial *Fh1* we performed serial transplantation assays. We transplanted 100 HSCs from FLs of *Fh1*$^{fl/fl}$;*FH*^{Cyt};*Vav-iCre*, *Fh1*$^{fl/fl}$*;Vav-iCre* and control 14.5 dpc embryos together with 200,000 support BM cells. While *Fh1*$^{fl/fl}$*;Vav-iCre* HSCs failed to repopulate the recipients, *Fh1*$^{fl/fl}$;*FH*^{Cyt};*Vav-iCre* HSCs contributed to primitive and more mature haematopoietic compartments of the recipient mice (Fig

3A). Primary recipients of *Fh1*$^{fl/fl}$;*FH*^{Cyt};*Vav-iCre* HSCs displayed efficient myeloid lineage reconstitution while B- and T-lymphoid lineage reconstitution was less robust (Fig. 3B), suggesting that mitochondrial Fh1 is required for lymphoid cell differentiation or survival. We next sorted BM LSK cells from the primary recipients and re-transplanted them into secondary recipients. *Fh1*$^{fl/fl}$*;FH*^{Cyt}*;Vav-iCre* HSCs failed to contribute to the BM haematopoietic compartments of the recipients 20 weeks after transplantation (Fig. 3C). Therefore, HSCs lacking mitochondrial Fh1 display progressive loss of self-renewal potential upon serial transplantation.

Haematopoietic defects upon *Fh1* deletion are not caused by oxidative stress or the activation of Nrf2-dependent pathways

Since elevated cellular fumarate is a major cause of haematopoietic defects in *Fh1*$^{fl/fl}$*;Vav-iCre* FLs, we next explored potential mechanisms through which fumarate impairs FL haematopoiesis. In non-haematopoietic tissues, fumarate succinates cysteine residues of biologically active molecules (including GSH (Sullivan et al., 2013; Zheng et al., 2015)) and numerous proteins (Adam et al., 2011; Ternette et al., 2013). Elevated fumarate causes oxidative stress by succinating glutathione (GSH) and thus generating succinicGSH and depleting the GSH pool (Sullivan et al., 2013; Zheng et al., 2015). We found that reactive oxygen species (ROS) were modestly increased in *Fh1*$^{fl/fl}$*;Vav-iCre* FL c-Kit^{+} cells compared to control cells (Fig. 4A). The quantity of succinicGSH was elevated in *Fh1*$^{fl/fl}$*;Vav-iCre* FL c-Kit^{+} cells (Fig. 4B) but succinicGSH constituted only approximately 1.5% of the total pool of glutathione species (Fig. 4C). Furthermore, we found that administration of the antioxidant N-acetyl cysteine (NAC) to timed-mated pregnant females did not rescue the reduced FL cellularity (data not shown), and failed to reverse decreased numbers of Lin^{+} FL cells (Fig. 4D). Finally, HSCs sorted from NAC-treated *Fh1*$^{fl/fl}$*;Vav-iCre* FLs failed to reconstitute haematopoiesis in NAC-treated recipient mice (Fig. 4E). Therefore, oxidative stress due to GSH depletion does not cause haematopoietic defects resulting from fumarate accumulation.

Loss of *Fh1* in renal cysts is associated with upregulation of Nrf2-mediated antioxidant response pathway due to fumarate-mediated succination of Keap1, which normally promotes Nrf2 degradation (Adam et al., 2011). However, the analyses of global gene expression profiling of FL $Lin^{-}c\text{-}Kit^{+}$ primitive haematopoietic cells from 14.5 dpc *Fh1*$^{fl/fl}$*;Vav-iCre* and control embryos revealed no significant enrichment for Nrf2 signature (Fig. 4F). Thus, the activation of the Nrf2-dependent pathways is not responsible for defective haematopoiesis in *Fh1*$^{fl/fl}$*;Vav-iCre* FLs.

***Fh1* deficiency in primitive haematopoietic cells has no impact on the Hif-1-dependent pathways and does not affect global 5-hydroxymethylcytosine levels**

Fumarate is known to competitively inhibit 2-oxoglutarate (2OG)-dependent oxygenases including Hif prolyl hydroxylase Phd2 resulting in stabilization of Hif-1α (Adam et al., 2011). Given that *Phd2* deletion and stabilization of Hif-1α results in HSC defects (Singh et al., 2013; Takubo et al., 2010), we asked whether elevated fumarate increases the Hif-1α protein levels upon *Fh1* deletion in primitive haematopoietic cells. We found that Hif-1α protein was undetectable in *Fh1*$^{fl/fl}$;*Vav-iCre* and control FL $c\text{-}Kit^{+}$ cells (Fig. 4G), and additional deletion of *Hif-1α* in *Fh1*-deficient embryos failed to rescue embryonic lethality (data not shown), restore total FL cellularity, reverse decreased FL Lin^{+} cell numbers or normalise elevated numbers of FL HSCs (Fig. 4H). Thus Hif-1α is not involved in generating haematopoietic defects in *Fh1*$^{fl/fl}$*;Vav-iCre* FLs. Given that fumarate can inhibit the Tet family of 5-methylcytosine hydroxylases (Xiao et al., 2012), we measured the levels of 5-hydroxymethylcytosine (5hmC) in *Fh1*$^{fl/fl}$*;Vav-iCre* and control $c\text{-}Kit^{+}$ cells and did not find any differences (data not shown), suggesting that fumarate-mediated Tet inhibition does not play a major role in generating haematopoietic defects in *Fh1*$^{fl/fl}$*;Vav-iCre* FLs.

***Fh1* deletion results in increased histone H3 trimethylation in primitive haematopoietic cells**

Emerging evidence indicates that 2OG-dependent JmjC domain-containing histone demethylases (KDMs) play important roles in HSC biology and haematopoiesis (Andricovich et al., 2016; Stewart et al., 2015). Given that fumarate inhibits enzymatic activity of KDMs (Xiao et al., 2012),

we examined the abundance of H3K4me3, H3K9me3, H3K27me3 and H3K36me3 in nuclear extracts from FL c-Kit^{+} cells isolated from 14.5 dpc *Fh1*$^{fl/fl}$*;Vav-iCre* and control embryos. Western blot analyses revealed an increase in levels of H3K9me3, H3K27me3 and H3K36me3 but not H3K4me3 in *Fh1*-deficient cells (Fig. 4I-J). While these data suggest that *Fh1* deficiency results in enhanced trimethylation of H3, the identity of KDMs that are inhibited by fumarate, and the causal roles for increased H3 trimethylation in mediating HSC and haematopoietic defects upon *Fh1* deletion remain to be elucidated.

***Fh1* deletion promotes a gene expression signature that facilitates haematopoietic defects**

In order to understand the molecular signatures associated with *Fh1* deficiency we performed gene expression profiling of FL Lin^{-}c-Kit^{+} primitive haematopoietic cells from *Fh1*$^{fl/fl}$*;Vav-iCre* and control embryos. We found that genes upregulated in *Fh1*-deficient cells are highly enriched in categories related to apoptosis in response to endoplasmic reticulum (ER) stress, protein metabolic process/protein translation and unfolded protein response (Fig. 4K-L). Downregulated genes are enriched in pathways related to haem biosynthesis, erythroid and myeloid function, and the cell cycle (Fig. 4K). Although further detailed work will be needed to experimentally verify this, we propose that enhanced ER stress, unfolded protein response and increased protein translation (which are known to contribute to HSC depletion and haematopoietic failure (Miharada et al., 2014; Signer et al., 2014; van Galen et al., 2014)) may be responsible for haematopoietic defects upon *Fh1* deletion.

***Fh1* deficiency abolishes leukaemic transformation and LIC functions**

While *FH* is a tumour suppressor (i.e. *FH* mutations result in hereditary leiomyomatosis and renal-cell cancer) and fumarate is proposed to function as an oncometabolite (Yang et al., 2013), the role of FH in leukaemic transformation remains unknown. Given that human AML cells express high levels of FH protein (Elo et al., 2014; Lopez-Pedrera et al., 2006) and enzymatic activity of FH is increased in AML samples compared to cells from normal controls (Tanaka and Valentine, 1961),

we next investigated the role for *Fh1* in leukaemic transformation. We employed a mouse model of AML in which the development and maintenance of leukaemia-initiating cells (LICs) is driven by *Meis1* and *Hoxa9* oncogenes (Vukovic et al., 2015; Wang et al., 2010). *Meis1* and *Hoxa9* are frequently overexpressed in several human AML subtypes (Drabkin et al., 2002; Lawrence et al., 1999) and their overexpression in mouse haematopoietic stem and progenitor cells generates self-renewing LICs (Kroon et al., 1998). In the *Meis1*/*Hoxa9* model employed here, the FL LSK or c-Kit^{+} cell populations are transduced with retroviruses expressing *Meis1* and *Hoxa9*, and are serially re-plated, generating a pre-leukaemic cell population which upon transplantation to primary recipients, develops into LICs causing AML. LICs are defined by their capacity to propagate AML with short latency in secondary recipients (Somervaille and Cleary, 2006; Vukovic et al., 2015; Yeung et al., 2010). We found that *Fh1*$^{fl/fl}$*;Vav-iCre* FL stem and progenitor cells transduced with *Meis1*/*Hoxa9* (Fig. 5A) failed to generate colonies in methylcellulose (Fig. 5B). To corroborate these findings, we used retroviruses expressing MLL fusions which are frequently found in acute monoblastic leukemia (AML M5) and are associated with an unfavourable prognosis in AML, namely *MLL-ENL* (fusion oncogene resulting from t(11;19)) and *MLL-AF9* (resulting from t(9;11)) (Krivtsov and Armstrong, 2007; Lavallee et al., 2015). We also used *AML1-ETO9a*, a splice variant of AML1-ETO that is frequently expressed in t(8;21) patients with AML M2 and its high expression correlates with poor AML prognosis (Jiao et al., 2009). MLL fusions and *AML1-ETO9a* drive leukaemogenesis through distinct pathways and are frequently used to transform murine haematopoietic cells (Smith et al., 2011; Velasco-Hernandez et al., 2014; Zuber et al., 2009). We found that *Fh1*-deficient cells transduced with *MLL-ENL*, *MLL-AF9* and *AML1-ETO9a* were unable to generate colonies (Fig. 5B), indicating the requirement for *Fh1* in *in vitro* transformation. We next determined the impact of *Fh1* deletion on the colony formation capacity of pre-leukaemic cells (Fig. 5C). We transduced *Fh1*$^{+/+}$ and *Fh1*$^{fl/fl}$ FL LSK cells with *Meis1* and *Hoxa9* retroviruses and following three rounds of re-plating we infected the transformed cells with *Cre* lentiviruses. *Fh1*$^{fl/fl}$

cells expressing *Cre* failed to generate colonies in CFC assays (Fig. 5D). Thus *Fh1* deletion inhibits the generation of pre-leukaemic cells and abolishes their clonogenic capacity.

To determine the requirement for *Fh1* in LICs, LSK cells from $Fh1^{+/+}$ and $Fh1^{fl/fl}$ FLs were transduced with *Meis1* and *Hoxa9* retroviruses, and transplanted into primary recipients (Fig. 5C). LICs isolated from leukaemic primary recipient mice were infected with *Cre* lentivirus and plated into methylcellulose. We found that *Fh1*-deficient LICs were unable to generate colonies (Fig. 5E). We next investigated the requirement for *FH* in human established leukaemic cells by knocking down the expression of *FH* in human AML (M5) THP-1 cells harbouring MLL-AF9 translocation. We generated lentiviruses expressing 3 independent short-hairpins (i.e. *FH* shRNA 1-3) targeting *FH*, and scrambled shRNA sequence. Based on knockdown efficiency (Fig. 5F-G) we selected *FH* shRNA1 and *FH* shRNA3 for further experiments. *FH* knockdown increased apoptosis of THP-1 cells (Fig. 5H) and decreased their ability to form colonies (Fig. 5I). Therefore, *Fh1* is required for survival of both mouse LICs and human established leukaemic cells. Finally, we conclude that the tumour suppressor functions of *FH* are tissue-specific and do not extend to haematopoietic cells.

Mitochondrial Fh1 is necessary for AML development but is not required for disease maintenance

We next investigated the impact of mitochondrial *Fh1* deficiency on *in vitro* transformation and development and maintenance of LICs (Fig. 6A-C). FL $Fh1^{fl/fl}$;FH^{Cyt};*Vav-iCre* cells transduced with *Meis1/Hoxa9* retroviruses had normal serial re-plating capacity (Fig. 6B), and the established pre-leukaemic cells had normal proliferative capacity and cell-cycle status (data not shown). Thus elevated fumarate is largely responsible for the inability of $Fh1^{fl/fl}$;*Vav-iCre* stem and progenitor cells to undergo *in vitro* transformation. To establish the requirement for mitochondrial *Fh1* in AML development *in vivo*, we transplanted control ($Fh1^{fl/fl}$), control;FH^{Cyt} and $Fh1^{fl/fl}$;FH^{Cyt};*Vav-iCre Meis1*/*Hoxa9*-transduced pre-leukaemic cells into sub-lethally irradiated recipient mice (Fig. 6A). We found that the percentage of recipients of $Fh1^{fl/fl}$;FH^{Cyt};*Vav-iCre* cells that developed

terminal AML was significantly reduced (and the disease latency was extended) compared to recipients of control and control;*FH*^{Cyt} cells (Fig. 6C). Finally, OCR measurement in LICs sorted from those recipients of *Fh1*$^{fl/fl}$*;FH*^{Cyt}*;Vav-iCre* cells that succumbed to AML revealed that *Fh1*$^{fl/fl}$*;FH*^{Cyt}*;Vav-iCre* LICs had defective maximal mitochondrial respiration compared to control and control;*FH*^{Cyt} LICs (data not shown). Thus mitochondrial *Fh1* is required for efficient generation of LICs and AML development in a *Meis1/Hoxa9*-driven model of leukaemogenesis.

Given that mitochondrial *Fh1* was important for leukaemia initiation, we next asked whether inducible deletion of mitochondrial *Fh1* from leukaemic cells impacts on leukaemia propagation and LIC maintenance (Fig. 6D-J). We transduced control and *Fh1*$^{fl/fl}$*;FH*^{Cyt}*;Mx1-Cre* FL LSK cells with *Meis1/Hoxa9* retroviruses and following serial re-plating the resultant pre-leukaemic cells were transplanted into primary recipient mice (Fig. 6D). Upon disease diagnosis (i.e. 20% of CD45.2^{+} leukaemic cells in the PB), the mice received 8 pIpC doses (Fig. 6D). Recipients of both control and *Fh1*$^{fl/fl}$*;FH*^{Cyt}*;Mx1-Cre* cells equally succumbed to terminal AML (Fig. 6E-F). After confirming efficient *Fh1* deletion (Fig. 6G) and defective maximal respiration (Fig. 6H), we isolated LICs from the BM of leukaemic primary recipient mice and transplanted them into secondary recipients. We found that LICs lacking mitochondrial *Fh1* and control LICs equally efficiently caused leukaemia in secondary recipients (Fig. 6I-J). Thus mitochondrial *Fh1* is necessary for efficient LIC generation but is not required for their ability to efficiently propagate *Meis1/Hoxa9*-driven leukaemia.

DISCUSSION

By performing genetic dissection of multifaceted functions of the key metabolic gene *Fh1* we have uncovered a previously unknown requirement for fumarate metabolism in the haematopoietic system. We conclude that efficient utilization of intracellular fumarate is required to prevent its potentially toxic effects and is central to the integrity of HSCs and haematopoietic differentiation. Furthermore, although fumarate promotes oncogenesis in the kidney (Yang et al., 2013), it has the

opposite effect in the haematopoietic system, i.e. it inhibits leukaemic transformation. Our data indicating a detrimental impact of fumarate on haematopoiesis, taken together with fumarate's functions as an oncometabolite in non-haematopoietic tumours (Yang et al., 2013), or a protective role within the myocardium (Ashrafian et al., 2012), highlight distinct functions of fumarate in different tissues.

Elevated fumarate within the haematopoietic system is likely to perturb multiple biochemical mechanisms. Fumarate is known to inhibit 2OG-dependent oxygenases, including HIF-hydroxylase Phd2 (Hewitson et al., 2007), the Tet enzymes and KDMs (Xiao et al., 2012) and as a consequence tumour cells with FH mutations have increased HIF-1α stability and display a hypermethylator phenotype (Castro-Vega et al., 2014; Isaacs et al., 2005; Letouze et al., 2013; Pollard et al., 2007). We found that haematopoietic defects resulting from elevated fumarate are most likely generated through the Hif-1-independent and Tet-independent mechanisms. However, consistent with the ability of fumarate to inhibit KDMs, we found that levels of H3K9me3, H3K27me3 and H3K36me3 were elevated in primitive haematopoietic cells lacking *Fh1*. Although detailed underlying mechanisms remain to be elucidated, we propose that elevated fumarate may cause the observed phenotypes by inhibiting these KDMs that are essential for normal haematopoiesis and HSC functions, including KDM5B (Stewart et al., 2015) and KDM2B (Andricovich et al., 2016).

Fumarate is also known to cause succination of cysteine residues of numerous proteins (e.g. Keap1, which normally promotes Nrf2 degradation (Adam et al., 2011; Ternette et al., 2013)) or GSH (Sullivan et al., 2013; Zheng et al., 2015). However, our data indicated that haematopoietic defects upon *Fh1* deletion are unlikely to be mediated by Nrf2 activation or GSH depletion. Given our findings that *Fh1*-deficient cells have increased signatures of ER stress and unfolded protein response, it will be of high interest to determine whether increased global protein succination in *Fh1*-deficient cells results in protein misfolding in HSCs, leading to the activation of unfolded protein response which is detrimental to HSC integrity (van Galen et al., 2014).

Fh1 deletion with the simultaneous re-expression of cytosolic FH allowed us to investigate the genetic requirement for mitochondrial *Fh1* in long-term HSC functions. Our serial transplantation assays revealed that mitochondrial Fh1 was essential for HSC self-renewal, indicating a key role for an intact TCA cycle in HSC maintenance. Intriguingly, while mitochondrial Fh1 deficiency did not affect myeloid output under steady-state conditions and upon transplantation, the lack of mitochondrial Fh1 had an impact on the lymphoid output. These data imply differential requirements for the intact TCA cycle in lineage commitment and/or differentiation of primitive haematopoietic cells, meriting further investigations.

Both self-renewing HSCs and LICs are thought to rely heavily on glycolysis while they suppress the TCA cycle (Simsek et al., 2010; Wang et al., 2014). We utilised the genetic mitochondrial *Fh1* deficiency to examine the differential requirement for mitochondrial Fh1 in long-term HSC self-renewal and the development and maintenance of LICs. We conclude that self-renewing HSCs critically require intact mitochondrial Fh1 and the capacity for maximal mitochondrial respiration to maintain their pool. However, while mitochondrial Fh1 was necessary for LIC development, it had no impact on maintenance of LICs. Thus we reveal a differential requirement for the mitochondrial TCA enzyme Fh1 in normal haematopoiesis and *Meis1/Hoxa9*-driven leukaemia propagation. The discovery of mechanisms underlying different metabolic requirements in HSCs and LICs represent a key area for future investigations.

MATERIALS AND METHODS

Mice

All mice were on the C57BL/6 genetic background. $Fh1^{fl/fl}$ (Pollard et al., 2007), $Hif\text{-}1\alpha^{fl/fl}$ (Ryan et al., 2000; Vukovic et al., 2016) and $V5\text{-}FH^{Cyt}$ (for simplicity referred to as FH^{Cyt}) (Adam et al., 2013) were described previously. *Vav-iCre* and *Mx1-Cre* were purchased from the Jackson Laboratory. All transgenic and knockout mice were $CD45.2^{+}$. Congenic recipient mice were

CD45.1$^+$/CD45.2$^+$. All experiments on animals were performed under UK Home Office authorisation.

Flow cytometry

All BM and FL samples were stained and analysed as described previously (Guitart et al., 2013; Kranc et al., 2009; Mortensen et al., 2011; Vukovic et al., 2016). BM cells were obtained by crushing tibias and femurs with a pestle and mortar. FL cells were obtained by mashing the tissue through a 70μm strainer. Single cell suspensions from BM, FL or PB were incubated with Fc block and then stained with antibodies. For HSC analyses, following incubation with Fc block, unfractionated FL or BM cell suspensions were stained with lineage markers containing biotin-conjugated anti-CD4, anti-CD5, anti-CD8a, anti-CD11b (not used in FL analyses), anti-B220, anti-Gr-1 and anti-Ter119 antibodies together with APC-conjugated anti-c-Kit, APC/Cy7-conjugated anti-Sca-1, PE-conjugated anti-CD48 and PE-Cy7-conjugated anti-CD150 antibodies. Biotin-conjugated antibodies were then stained with Pacific Blue-conjugated or PerCP-conjugated streptavidin. To distinguish CD45.2$^+$-donor derived HSCs in recipient mice, FITC-conjugated anti-CD45.1 and Pacific Blue-conjugated anti-CD45.2 antibodies were included in the antibody cocktail described above. The multilineage reconstitution of recipient mice was determined by staining the BM or PB cell suspensions of the recipient mice with FITC-conjugated anti-CD45.1, Pacific Blue-conjugated anti-CD45.2, PE-conjugated anti-CD4 and-CD8a, PE/Cy7-conjugated anti-Gr-1, APC-conjugated anti-CD11b, APC-Cy7-conjugated anti-CD19 and anti-B220). In all analyses, 7-AAD or DAPI were used for dead cell exclusion.

Flow cytometry analyses were performed using a LSRFortessa (BD). Cell sorting was performed on a FACSAria Fusion (BD).

Colony forming cells (CFC) assays

CFC assays were performed using MethoCult^{TM} M3434 (STEMCELL Technologies). Two replicates were used per group in each experiment. Colonies were tallied at day 10.

Leukaemic transformation

LSK cells were sorted from FLs of 14.5 dpc embryos following c-Kit (CD117) enrichment using MACS columns (Miltenyi Biotec). 10,000 LSK cells were simultaneously transduced with MSCV-*Meis1a-puro* and MSCV-*Hoxa9-neo* retroviruses and subsequently subjected to three rounds of CFC assays in MethoCult^{TM} M3231 (STEMCELL Technologies) supplemented with 20ng/ml SCF, 10ng/ml IL-3, 10ng/ml IL-6 and 10ng/ml GM-SCF. Colonies were counted 6-7 days after plating, and 2,500 cells were re-plated. Similarly, 200,000 FL c-Kit^{+} cells were transduced with MSCV-*AML1-ETO9a-neo,* MSCV-*MLL-AF9-neo* or MSCV-*MLL-ENL-neo* and subsequently plated into methylcellulose.

Transplantation assays

Lethal irradiation of CD45.1^{+}/CD45.2^{+} recipient mice was achieved using a split dose of 11 Gy (two doses of 5.5 Gy administered at least 4 hours apart) at an average rate of 0.58 Gy/min using a Cesium 137 GammaCell 40 irradiator. For sub-lethal irradiation, the recipient mice received a split dose of 7 Gy (two doses of 3.5 Gy, at least 4 hours apart).

For primary transplantations 100 HSCs (LSKCD48^{-}CD150^{+}CD45.2^{+}) sorted from FLs of 14.5 dpc embryos or 200,000 unfractionated FL cells were mixed with 200,000 support CD45.1^{+} BM cells and injected into lethally irradiated (11 Gy delivered in a split dose) CD45.1^{+}/CD45.2^{+} recipient mice. For secondary transplantations 2,000 CD45.2^{+} LSK cells sorted from BM of primary recipients were mixed with 200,000 support CD45.1^{+} wild-type BM cells and re-transplanted. For adult BM transplantations 500,000 CD45.2^{+} BM cells were mixed with 500,000 support CD45.1^{+} wild-type BM cells and injected into lethally irradiated CD45.1^{+}/CD45.2^{+} recipient mice. All recipient mice were analysed 18-20 weeks post-transplantation, unless otherwise stated.

For leukaemia induction, 100,000 *Meis-1*/*Hoxa9*-transduced c-Kit^{+} cells were transplanted into CD45.1^{+}/CD45.2^{+} sub-lethally irradiated (7 Gy delivered in a split dose) recipient mice. The mice were monitored for AML development. For secondary transplantation, 10,000 LICs (CD45.2^{+}c-Kit^{+}

cells) were sorted from BM of primary recipients and transplanted into secondary $CD45.1^+/CD45.2^+$ sub-lethally irradiated recipient mice.

Inducible *Mx1-Cre*-mediated gene deletion

Mice were injected intraperitoneally 6-8 times every alternate day with 300 µg pIpC (GE Healthcare) as previously described (Guitart et al., 2013; Kranc et al., 2009).

Administration of N-acetylcysteine (NAC)

Pregnant females received 30 mg/mL of NAC (Sigma-Aldrich) in drinking water (pH was adjusted to 7.2-7.4 with NaOH). For transplantation experiments, $CD45.1^+/CD45.2^+$ recipient mice were treated with 30 mg/mL NAC in drinking water 7 days prior to irradiation, and remained under NAC treatment for the duration of the experiment. The water bottle containing NAC was changed twice a week.

Oxygen consumption assays

Oxygen consumption rate (OCR) measurements were made using a Seahorse XF-24 analyser (Seahorse Bioscience) and the XF Cell Mito Stress Test Kit as previously described (Wang et al., 2014). Briefly, c-Kit^+ cells from FLs of 14.5 dpc embryos were plated in XF-24 microplates pre-coated with cell-tak (BD) at 250,000 cells per well in XF Base Medium supplemented with 2 mM pyruvate and 10 mM glucose (pH 7.4). OCR was measured 3 times every 6 min for basal value and after each sequential addition of oligomycin (1µM), FCCP (1µM) and finally concomitant rotenone and antimycin A (1µM). 1µM FCCP was used as at this concentration FCCP elicited maximal fold increase in OCR (data not shown). Oxygen consumption measurements were normalised to cell counts performed before and after each assay.

Metabolite detection by LC-MS

Metabolites from c-Kit^+ cells from FLs of 14.5 dpc embryos were extracted into 50% methanol/30% acetonitrile and measured as previously described (Adam et al., 2013).

Western blotting

Protein extracted from FL c-Kit$^+$ cells of 14.5 dpc embryos was subjected to a 10% SDS–PAGE then transferred onto a PVDF membrane and immunoblotted with anti-Fh1, anti-2-SC and anti-Hif-1α as previously described (Adam et al., 2011; Bardella et al., 2012). Anti-H3K4me3 (07-473; Millipore), anti-H3K9me3 (ab8898; Abcam), anti-H3K27me3 (07-449; Millipore), anti-H3K36me3 (ab9050; Abcam) were used to determine levels of trimethylated H3. Anti-actin (A5316; Sigma), anti-tubulin (2146S; Cell signalling) and anti-H3 (ab1791; Abcam) immunoblots were used as loading controls.

RT-qPCR

Gene expression analyses were performed as described previously (Guitart et al., 2013; Kranc et al., 2009; Mortensen et al., 2011). Differences in input cDNA were normalised with *Actb* (beta actin) expression.

ATP production

10,000 c-Kit$^+$ cells from FLs of 14.5 dpc embryos were cultured in DMEM supplemented with either 25mM glucose or 25mM galactose. At 0 and 24 hours after incubation the cells were lysed and ATP content was measured by luminescence using CellTiterGlo Assay (Promega).

Measurement of mitochondrial membrane potential

50,000 FL c-Kit$^+$ cells from 14.5 dpc embryos were incubated for 15min at 37°C in 25nM TMRM (T-668, Life Technologies) and analysed using the LSRFortessa flow cytometer.

Gene expression profiling and bioinformatics analyses

RNA from sorted FL Lin$^-$c-Kit$^+$ cells was isolated by standard phenol/chloroform extraction. cDNA was synthesised from 50ng of total RNA using the Ambion WT Expression kit (Life Technologies). Labeled, fragmented cDNA (Affymetrix GeneChip® WT Terminal Labeling and Controls Kit) was hybridized to Mouse Gene 2.0 arrays for 16 hours at 45°C (at 60rpm) (Affymetrix GeneChip® Hybridization, Wash, and Stain Kit). Arrays were washed and stained using the Affymetrix Fluidics

Station 450, and scanned using the Hewlett-Packard GeneArray Scanner 3000 7G. The microarray gene expression data have been deposited in ArrayExpress (accession number E-MTAB-5425).

For bioinformatics analyses, a total of 7 arrays (n = 3 *Fh1*$^{fl/fl}$, n = 4 *Fh1*$^{fl/fl}$;*Vav-iCre*) were QC (quality control) analysed using arrayQualityMetrics package in Bioconductor. Normalisation of the 29638 features across all arrays was achieved using the robust multi-array average (RMA) expression measure. Pairwise group comparisons were undertaken using linear modelling (LIMMA package in Bioconductor). Subsequently, empirical Bayesian analysis was applied, including vertical (within a given comparison) p-value adjustment for multiple testing, which controls for false-discovery rate.

Gene set enrichment analysis

Gene expression differences were ranked by difference of log expression values, and this ranking was used to perform gene set enrichment analysis (GSEA) (Subramanian et al., 2005) on gene lists in the Molecular signatures database (MSigDB, version 5.2). The following datasets were used for analyses presented in Fig. 4: 1) Hallmark, unfolded protein response; 2) GO, Intrinsic apoptotic signalling pathway in response to endoplasmic reticulum stress; 3) Reactome, translation; and 4) NFE2L2.V2.

shRNA-dedicated *FH* knockdown

THP-1 cells were transduced with lentiviruses expressing shRNAs (shRNA1: TAATCCTGGT TTACTTCAGCG (TRCN0000052463), shRNA2: AAGGTATCATATTCTATCCGG (TRCN0000052464), shRNA3: TTTATTAACATGATCGTTGGG (TRCN0000052465) and shRNA Scr: TTCTCCGAACGTGTCACGTT; Dharmacon™RNAi Consortium). Transduced THP-1 cells were grown in the presence of 5ug/mL puromycin.

ROS analysis

c-Kit^{+} cells were stained with 2.5nM CellROX (C10491, Life Technologies) based on the manufacturer's protocol and analysed by FACS.

Statistical analyses

Statistical analyses were performed using GraphPad Prism 6 software (GraphPad Software, Inc.) P values were calculated using a two-tailed Mann–Whitney U test unless stated otherwise. Kaplan-Meier survival curve statistics were determined using the Log-rank (Mantel Cox) test.

ACKNOWLEDGMENTS

K.R.K. is a Cancer Research UK Senior Cancer Research Fellow. This project was funded by The Kay Kendall Leukaemia Fund, Cancer Research UK, Bloodwise, Tenovus Scotland, and The Wellcome Trust. We thank Dr. Vladimir Benes and Jelena Pistolic from the Genomics Core facility of the European Molecular Biology Laboratory (Heidelberg) for performing the gene expression profiling.

The authors declare no competing financial interests.

Figure Legends

Figure 1. Haematopoiesis-specific *Fh1* deletion results in severe haematopoietic defects and loss of HSC activity. (A) Relative levels of *Fh1* mRNA (normalised to *Actb*) in HSCs, MPPs, HPC-1 and HPC-2 populations, LSK and LK cells sorted from 14.5 dpc FLs and BM of C57BL/6 adult (8-10 week old) mice. Data are mean ± s.e.m. (n = 3). (B) FLs from 14.5 dpc *Fh1*$^{fl/fl}$;*Vav-iCre* embryos are smaller and paler compared to *Fh1*$^{+/fl}$;*Vav-iCre* and control embryos. (C) The absence of *Fh1* transcripts in *Fh1*$^{fl/fl}$;*Vav-iCre* FL CD45$^+$ and c-Kit$^+$ cells. Data are mean ± s.e.m. (control n = 3 and *Fh1*$^{fl/fl}$;*Vav-iCre* n = 6). (D) Western blots for Fh1 and β-actin in FL c-Kit$^+$ cells. (E) Total cellularity (the sum of Lin$^+$ and Lin$^-$ cell numbers) in 14.5 dpc FLs of the indicated genotypes. Data are mean ± s.e.m. (control n = 17, *Fh1*$^{+/fl}$;*Vav-iCre* n = 11, *Fh1*$^{fl/fl}$;*Vav-iCre* n = 9). (F) CFC assay with FL cells. Data are mean ± s.e.m. (control n = 11, *Fh1*$^{+/fl}$;*Vav-iCre* n = 8, *Fh1*$^{fl/fl}$;*Vav-iCre* n = 4). (G) Erythropoiesis in 14.5 dpc FLs. Arranged from least to most differentiated, Ter119$^-$CD71$^-$, Ter119$^-$CD71$^+$, Ter119$^+$CD71$^+$ and Ter119$^+$CD71$^-$. Data are mean ± s.e.m. (control n = 11, *Fh1*$^{+/fl}$;*Vav-iCre* n = 8, *Fh1*$^{fl/fl}$;*Vav-iCre* n = 4). (H-J) Total number of LK cells (H), LSK cells (I) and HSCs (J) in 14.5 dpc FLs. Data are mean ± s.e.m. (control n = 17, *Fh1*$^{+/fl}$;*Vav-iCre* n = 11, *Fh1*$^{fl/fl}$;*Vav-iCre* n = 9). (K-L) Percentage of donor-derived CD45.2$^+$ cells in PB (K), and total BM and the BM LSK cell compartment (L) of the recipient mice transplanted with 100 FL HSCs. Data are mean ± s.e.m.; n = 5-8 recipients per genotype, at least 3 donors were used per genotype. (M) Percentage of CD45.2$^+$ cells in PB after transplantation of 200,000 total FL cells. Data are mean ± s.e.m.; n = 3-4 recipients per genotype, at least 3 donors were used per genotype. (N-O) Acute deletion of *Fh1* from the adult haematopoietic system. 5x10^5 unfractionated CD45.2$^+$ BM cells from untreated *Fh1*$^{fl/fl}$ (control), *Fh1*$^{+/fl}$*;Mx1-Cre* and *Fh1*$^{fl/fl}$*;Mx1-Cre* C57BL/6 (8-10 week old) mice were mixed with 5x10^5 CD45.1$^+$ WT BM cells and transplanted into lethally irradiated CD45.1$^+$/CD45.2$^+$ recipients. 8 weeks after transplantation, the recipients received 6 doses of pIpC. (N) Percentage of donor-derived CD45.2$^+$ cells in PB (n = 5-10 recipients per genotype; n = 2 donors per genotype). (O) Percentage of CD45.2$^+$ cells in the Lin$^+$, Lin$^-$, LK, LSK and HSC cell

compartments of the recipient mice 11 weeks after pIpC treatment. Data are mean ± s.e.m. (*n* = 7-8 recipients per genotype). (C, E, F-G, and J-O) *, P < 0.05; **, P < 0.01; ***, P < 0.001; ****, P < 0.0001 (Mann-Whitney U test).

Figure 2. Cytosolic isoform of *Fh1* restores normal steady-state haematopoiesis in *Fh1*$^{fl/fl}$;*Vav-iCre* mice. (A) OCR in FL c-Kit^{+} cells under basal conditions and following the sequential addition of oligomycin, FCCP, and rotenone and antimycin A. Data are mean ± s.e.m. (control *n* = 5, *Fh1*$^{fl/fl}$;*Vav-iCre* *n* = 3, control;*FH*^{Cyt} *n* = 10, *Fh1*$^{fl/fl}$;*FH*^{Cyt};*Vav-iCre* *n* =5). (B) OXPHOS-dependent ATP production in galactose (Gal)-treated FL c-Kit^{+} *Fh1*$^{fl/fl}$;*Vav-iCre* and *Fh1*$^{fl/fl}$;*FH*^{Cyt};*Vav-iCre* cells. Control (*n* = 9), *Fh1*$^{fl/fl}$;*Vav-iCre* (*n* = 9), control;*FH*^{Cyt} (*n* = 6), *Fh1*$^{fl/fl}$;*FH*^{Cyt};Vav-iCre (*n* = 10). FL c-Kit^{+} cells were cultured in DMEM supplemented with either 25 mM glucose (Glu) or 25 mM Gal. The graph shows the ratio of ATP produced in the presence of Gal (permissive for oxidative phosphorylation only) to ATP generated in the presence of Glu (permissive for both oxidative phosphorylation and glycolysis). Data are mean ± s.e.m. (control *n* = 9, *Fh1*$^{fl/fl}$;*Vav-iCre* *n* = 10, control;*FH*^{Cyt} *n* =6, *Fh1*$^{fl/fl}$;*FH*^{Cyt};Vav-iCre *n* = 9). (C) Relative expression (normalised to *Actb*) of genes involved in glycolysis in FL c-Kit^{+} cells. Data are mean ± s.e.m.; *n* = 4-5 per genotype. (D) ECAR under basal conditions in 14.5 dpc FL c-Kit^{+} cells. Data are mean ± s.e.m. (control *n* = 6, *Fh1*$^{fl/fl}$;*Vav-iCre* *n* = 5, control;*FH*^{Cyt} *n* =10, *Fh1*$^{fl/fl}$;*FH*^{Cyt};Vav-iCre *n* = 4). (E) Fumarate and (F) argininosuccinate levels in FL c-Kit^{+} cells measured using LC-MS. Data are mean ± s.e.m. (control *n* = 6, *Fh1*$^{fl/fl}$;*Vav-iCre* *n* = 4, control;*FH*^{Cyt} *n* = 6, *Fh1*$^{fl/fl}$;*FH*^{Cyt};*Vav-iCre* *n* = 13). (G) 14.5 dpc FL cell extracts were immunoblotted with a polyclonal anti-2SC antibody. α-tubulin was used as a loading control. Data are representative of two independent experiments. (H) Colony forming unit (CFU) assays performed with BM cells from 8-10 week old mice of the indicated genotypes. CFU-erythroid and/or megakaryocyte (Red); CFU-granulocyte (G); CFU-monocyte/macrophage (M) CFU-granulocyte and monocyte/macrophage (GM); CFU-mix, at least three of the following: G, E, M and Mk. Data are mean ± s.e.m. (*n* = 3-5 per genotype) and are representative of 3 independent experiments. (I) Total number of BM nucleated cells

obtained from 2 tibias and 2 femurs of 8-10 week old mice. Data are mean ± s.e.m. (n = 3-4 per genotype). (J-N) Total numbers of $CD11b^{+}Gr\text{-}1^{+}$ myeloid cells (J), $CD19^{+}B220^{+}$ B cells (K), LK cells (L), LSK cells (M), and HSCs (N) in 2 tibias and 2 femurs. Data are mean ± s.e.m. (n = 3-4 per genotype). (A-F, H, K, M-N) *, $P < 0.05$; **, $P < 0.01$; ***, $P < 0.001$; ****, $P < 0.0001$ (Mann-Whitney U test).

Figure 3. Mitochondrial *Fh1* is essential for HSC self-renewal. 100 FL HSCs were transplanted into lethally irradiated 8-10 week old C57BL/6 $CD45.1^{+}/CD45.2^{+}$ recipient mice together with $2x10^{5}$ $CD45.1^{+}$ syngeneic competitor BM cells. The primary recipients were analysed 20 weeks after transplantation. 2,000 $CD45.2^{+}$LSK cells were sorted from their BM and transplanted into secondary recipients together with competitor BM cells. Secondary recipients were analysed 20 weeks after transplantation. (A) Percentage of $CD45.2^{+}$ cells in the Lin^{+}, Lin^{-}, LK, LSK and HSC compartments in the BM of primary recipients. Data are mean ± s.e.m.; n = 4-5 recipients per donor (B) Percentage of $CD45.2^{+}$ cells in the monocyte, neutrophil, B cell and T cell compartments in the PB of primary recipients. Data are mean± s.e.m. (n = 4-5 recipients per donor). Number of donors used in (A) and (B): control n = 6, $Fh1^{+/fl}$;*Vav-iCre* n = 2, $Fh1^{fl/fl}$;*Vav-iCre* n = 2, control;FH^{Cyt} n = 6, $Fh1^{+/fl}$;FH^{Cyt};*Vav-iCre* n = 3, $Fh1^{fl/fl}$;FH^{Cyt};*Vav-iCre* n = 3). (C) Percentage of $CD45.2^{+}$ cells in the Lin^{+}, Lin^{-}, LK, LSK and HSC compartments in the BM of the secondary recipients. Data are mean ± s.e.m. n = 4-5 recipients per donor (number of donors: control n = 3, control;FH^{Cyt} n = 4, $Fh1^{+/fl}$;FH^{Cyt};*Vav-iCre* n = 2 and $Fh1^{fl/fl}$;FH^{Cyt};*Vav-iCre* n = 3). (A-C) *, $P < 0.05$; **, $P < 0.01$ (Mann-Whitney U test).

Figure 4. Molecular consequences of *Fh1* deletion in primitive haematopoietic cells. (A) Intracellular ROS in FL $c\text{-}Kit^{+}$ cells. Data are the mean of mean fluorescence intensities ± s.e.m. (control n = 6 and $Fh1^{fl/fl}$;*Vav-iCre* n = 3). (B-C) Glutathione species in 14.5 dpc FL $c\text{-}Kit^{+}$ cells measured using LC-MS. (B) SuccinicGSH levels (arbitrary units) and (C) percentage of SuccinicGSH within the total glutathione species. Data are mean ± s.e.m. (control n = 6 and

Fh1$^{fl/fl}$;*Vav-iCre* n = 3). (D-E) Pregnant females were treated with NAC administered 7 days prior to the embryo harvest. (D) Lin$^+$ cell numbers in 14.5 dpc FLs. Data are mean ± s.e.m. (control n = 15, *Fh1*$^{fl/fl}$;*Vav-iCre* n = 6, control + NAC n = 4 and *Fh1*$^{fl/fl}$;*Vav-iCre* + NAC n = 4). (E) 600,000 total FL cells of 14.5 dpc embryos from NAC-treated pregnant females, were transplanted into lethally irradiated CD45.1$^+$/CD45.2$^+$ recipient mice together with 200,000 CD45.1$^+$ competitor BM cells. Recipients were continuously treated with NAC. Data represent percentage of donor-derived CD45.2$^+$ cells in PB 3 weeks post-transplantation (n = 10-11 recipients per genotype; n = 4 donors per genotype). (F) Gene set enrichment analysis (GSEA) showing that the Nrf2 signature is not significantly affected in *Fh1*-deficient (*Fh1* KO) FL Lin$^-$c-Kit$^+$ cells. NES: normalized enrichment score; FDR: false discovery rate. (G) Western blots for Hif-1α and β-actin in c-Kit$^+$ cells from 14.5 dpc FLs (n = 3 per genotype). $CoCl_2$-treated FL c-Kit$^+$ cells were used as a positive control for Hif-1α. Asterisks indicate nonspecific bands. (H) Total FL cellularity and total number of Lin$^+$ cells and HSCs in 14.5 dpc FLs. Data are mean ± s.e.m. (*Fh1*$^{fl/fl}$;*Hif-1α*$^{+/+}$ n = 12, *Fh1*$^{fl/fl}$;*Hif-1α*$^{+/+}$;*Vav-iCre* n = 9, *Fh1*$^{fl/fl}$;*Hif-1α*$^{fl/fl}$ n = 6, *Fh1*$^{+/fl}$;*Hif-1α*$^{fl/fl}$;*Vav-iCre* n = 5, *Fh1*$^{fl/fl}$;*Hif-1α*$^{fl/fl}$;*Vav-iCre* n = 4). (I) Western blot for H3K4me3, H3K9me3, H3K27me3, H3K36me3 and total H3 in 14.5 dpc FL c-Kit$^+$ cells (n = 3 per genotype). (J) Quantification of the data (normalized to total H3) shown in panel I. Mean ± s.e.m. (K) Biological processes (presented as –log10 (P-value)) that are enriched in up-regulated and down-regulated genes in *Fh1*-deficient FL Lin$^-$c-Kit$^+$ cells versus control cells. Analysis was performed using the Gene Ontology Consortium database. The dashed grey line indicates P = 0.05. (L) Signature enrichment plots from GSEA analyses using unfolded protein response, apoptosis in response to ER stress and protein translation signature gene sets. (F, K-L) Gene expression analysis was preformed using Lin$^-$c-Kit$^+$ cells from 3 *Fh1*$^{fl/fl}$ (WT) and 4 *Fh1*$^{fl/fl}$;*Vav-iCre* (*Fh1* KO) embryos. (A-E, H, J) *, P < 0.05; **, P < 0.01; ***, P< 0.001; ****, P < 0.0001 (Mann-Whitney U test).

Figure 5. *Fh1* is required for leukaemic transformation. (A) 14.5 dpc FL c-Kit$^+$ cells were transduced with *Meis1*/*Hoxa9*, *MLL-AF9*, *MLL-ENL* and *AML1-ETO9a* retroviruses and plated into

methylcellulose. (B) Colony counts (mean ± s.e.m.) 6 days after plating are shown. *n* = 4-5 per genotype. (C) *Fh1*$^{+/+}$ and *Fh1*$^{fl/fl}$ (without *Vav-iCre*) FL LSK cells were co-transduced with *Meis1* and *Hoxa9* retroviruses and serially re-plated. The cells were subsequently infected with a bicistronic lentivirus expressing *iCre* and a Venus reporter. Venus^{+} cells were plated into methylcellulose. In parallel, *Fh1*$^{+/+}$ and *Fh1*$^{fl/fl}$ pre-leukaemic cells were transplanted into recipient mice. LICs (CD45.2^{+}c-Kit^{+} cells) were sorted from the BM of leukaemic recipients, transduced with *Cre* lentivirus and plated into methylcellulose. (D) Number of colonies generated by *Cre*-expressing pre-leukaemic cells. Data are mean ± s.e.m., *n* = 3 per genotype. (E) Number of colonies generated by *Cre*-expressing LICs. Data are mean ± s.e.m., *n* = *3* per genotype. (F) Relative levels of *FH* mRNA (normalised to *ACTB*) in untransduced THP-1 cells and THP-1 cells transduced with lentiviruses expressing scrambled shRNA (Scr shRNA) and 3 different shRNAs targeting *FH* (FH shRNA1, FH shRNA2 and FH shRNA3). Data are mean ± s.e.m., *n* = 3. (G) Western blot for FH and β-actin in THP-1 cells described in Fig. 5F. (H) Apoptosis assays performed with THP-1 cells transduced with lentiviruses expressing Scr shRNA, FH shRNA1 and FH shRNA3. The graph depicts the percentage of Annexin V^{+}DAPI$^{–}$ cells in early apoptosis and Annexin V^{+}DAPI^{+} in late apoptosis. Data are mean ± s.e.m., *n* = 4. (I) CFC assays with THP-1 cells expressing Scr shRNA, FH shRNA1 and FH shRNA3. Mean ± s.e.m., *n* = 5. (H-I) *, P < 0.05 (Mann-Whitney U test).

Figure 6. Mitochondrial Fh1 is necessary for efficient leukaemia establishment but is not required for AML propagation. (A) Control, *Fh1*$^{fl/fl}$;*FH*^{Cyt} (i.e. Control;*FH*^{Cyt}) and *Fh1*$^{fl/fl}$;*FH*^{Cyt};*Vav-iCre* FL LSK cells were co-transduced with *Meis1* and *Hoxa9* retroviruses and serially re-plated. 100,000 c-Kit^{+} pre-leukaemic cells were transplanted into sub-lethally irradiated recipient mice. (B) CFC counts at each re-plating. Data are mean ± s.e.m., *n* = 6-8 per genotype. (C) Kaplan-Meier survival curve of primary recipient mice (*n* = 8-10 recipients per genotype; 4 donors per genotype). ***, P < 0.001 Log-rank (Mantel-Cox). (D) Control and *Fh1*$^{fl/fl}$;*FH*^{Cyt};*Mx1-Cre* FL LSK cells were co-transduced with *Meis1* and *Hoxa9* retroviruses and serially re-plated. The resultant pre-leukaemic cells were transplanted into sub-lethally irradiated recipients. Once

leukaemic CD45.2$^+$ cells reached 20% in the PB of recipient mice, the recipients received 8 doses of pIpC. 10,000 LICs (CD45.2$^+$c-Kit$^+$) from primary recipients were transplanted into secondary recipients. (E) Kaplan-Meier survival curve of primary recipient mice. pIpC treatment was initiated 5 weeks post transplantation (n = 5-7 recipients per genotype). (F) Percentage of CD45.2$^+$ cells in BM of primary recipient mice with terminal leukaemia. Data are mean ± s.e.m., n = 5-7 recipients per genotype. (G) Genomic PCR assessing *Fh1* deletion before pIpC (top) and after pIpC (bottom) treatment. fl – undeleted conditional allele; Δ – excised allele. (H) OCR in LICs isolated from the BM of primary recipients treated with pIpC. OCR was assayed as described in Fig 2A. Data are mean ± s.e.m., n = 3-5. *, $P < 0.05$ (Mann-Whitney U test). (I) Kaplan-Meier survival curve of secondary recipients transplanted with LICs sorted from leukaemic primary recipients ($n = 10$ per genotype). (J) Representative gel showing PCR amplification of genomic DNA from the total BM of secondary recipients with terminal leukaemia.

References

Adam, J., E. Hatipoglu, L. O'Flaherty, N. Ternette, N. Sahgal, H. Lockstone, D. Baban, E. Nye, G.W. Stamp, K. Wolhuter, M. Stevens, R. Fischer, P. Carmeliet, P.H. Maxwell, C.W. Pugh, N. Frizzell, T. Soga, B.M. Kessler, M. El-Bahrawy, P.J. Ratcliffe, and P.J. Pollard. 2011. Renal cyst formation in Fh1-deficient mice is independent of the Hif/Phd pathway: roles for fumarate in KEAP1 succination and Nrf2 signaling. *Cancer Cell* 20:524-537.

Adam, J., M. Yang, C. Bauerschmidt, M. Kitagawa, L. O'Flaherty, P. Maheswaran, G. Ozkan, N. Sahgal, D. Baban, K. Kato, K. Saito, K. Iino, K. Igarashi, M. Stratford, C. Pugh, D.A. Tennant, C. Ludwig, B. Davies, P.J. Ratcliffe, M. El-Bahrawy, H. Ashrafian, T. Soga, and P.J. Pollard. 2013. A role for cytosolic fumarate hydratase in urea cycle metabolism and renal neoplasia. *Cell Rep* 3:1440-1448.

Alderson, N.L., Y. Wang, M. Blatnik, N. Frizzell, M.D. Walla, T.J. Lyons, N. Alt, J.A. Carson, R. Nagai, S.R. Thorpe, and J.W. Baynes. 2006. S-(2-Succinyl)cysteine: a novel chemical modification of tissue proteins by a Krebs cycle intermediate. *Arch Biochem Biophys* 450:1-8.

Andricovich, J., Y. Kai, W. Peng, A. Foudi, and A. Tzatsos. 2016. Histone demethylase KDM2B regulates lineage commitment in normal and malignant hematopoiesis. *J Clin Invest* 126:905-920.

Ashrafian, H., G. Czibik, M. Bellahcene, D. Aksentijevic, A.C. Smith, S.J. Mitchell, M.S. Dodd, J. Kirwan, J.J. Byrne, C. Ludwig, H. Isackson, A. Yavari, N.B. Stottrup, H. Contractor, T.J. Cahill, N. Sahgal, D.R. Ball, R.I. Birkler, I. Hargreaves, D.A. Tennant, J. Land, C.A. Lygate, M. Johannsen, R.K. Kharbanda, S. Neubauer, C. Redwood, R. de Cabo, I. Ahmet, M. Talan, U.L. Gunther, A.J. Robinson, M.R. Viant, P.J. Pollard, D.J. Tyler, and H. Watkins. 2012. Fumarate is cardioprotective via activation of the Nrf2 antioxidant pathway. *Cell Metab* 15:361-371.

Bardella, C., M. El-Bahrawy, N. Frizzell, J. Adam, N. Ternette, E. Hatipoglu, K. Howarth, L. O'Flaherty, I. Roberts, G. Turner, J. Taylor, K. Giaslakiotis, V.M. Macaulay, A.L. Harris, A. Chandra, H.J. Lehtonen, V. Launonen, L.A. Aaltonen, C.W. Pugh, R. Mihai, D. Trudgian, B. Kessler, J.W. Baynes, P.J. Ratcliffe, I.P. Tomlinson, and P.J. Pollard. 2011. Aberrant succination of proteins in fumarate hydratase-deficient mice and HLRCC patients is a robust biomarker of mutation status. *J Pathol* 225:4-11.

Bardella, C., M. Olivero, A. Lorenzato, M. Geuna, J. Adam, L. O'Flaherty, P. Rustin, I. Tomlinson, P.J. Pollard, and M.F. Di Renzo. 2012. Cells lacking the fumarase tumor suppressor are protected from apoptosis through a hypoxia-inducible factor-independent, AMPK-dependent mechanism. *Mol Cell Biol* 32:3081-3094.

Bourgeron, T., D. Chretien, J. Poggi-Bach, S. Doonan, D. Rabier, P. Letouze, A. Munnich, A. Rotig, P. Landrieu, and P. Rustin. 1994. Mutation of the fumarase gene in two siblings with progressive encephalopathy and fumarase deficiency. *J Clin Invest* 93:2514-2518.

Castro-Vega, L.J., A. Buffet, A.A. De Cubas, A. Cascon, M. Menara, E. Khalifa, L. Amar, S. Azriel, I. Bourdeau, O. Chabre, M. Curras-Freixes, V. Franco-Vidal, M. Guillaud-Bataille, C. Simian, A. Morin, R. Leton, A. Gomez-Grana, P.J. Pollard, P. Rustin, M. Robledo, J. Favier, and A.P. Gimenez-Roqueplo. 2014. Germline mutations in FH confer predisposition to malignant pheochromocytomas and paragangliomas. *Hum Mol Genet* 23:2440-2446.

Choi, S.W., A.A. Gerencser, and D.G. Nicholls. 2009. Bioenergetic analysis of isolated cerebrocortical nerve terminals on a microgram scale: spare respiratory capacity and stochastic mitochondrial failure. *J Neurochem* 109:1179-1191.

de Boer, J., A. Williams, G. Skavdis, N. Harker, M. Coles, M. Tolaini, T. Norton, K. Williams, K. Roderick, A.J. Potocnik, and D. Kioussis. 2003. Transgenic mice with hematopoietic and lymphoid specific expression of Cre. *Eur J Immunol* 33:314-325.

Drabkin, H.A., C. Parsy, K. Ferguson, F. Guilhot, L. Lacotte, L. Roy, C. Zeng, A. Baron, S.P. Hunger, M. Varella-Garcia, R. Gemmill, F. Brizard, A. Brizard, and J. Roche. 2002. Quantitative HOX expression in chromosomally defined subsets of acute myelogenous leukemia. *Leukemia* 16:186-195.

Elo, L.L., R. Karjalainen, T. Ohman, P. Hintsanen, T.A. Nyman, C.A. Heckman, and T. Aittokallio. 2014. Statistical detection of quantitative protein biomarkers provides insights into signaling networks deregulated in acute myeloid leukemia. *Proteomics* 14:2443-2453.

Ferrick, D.A., A. Neilson, and C. Beeson. 2008. Advances in measuring cellular bioenergetics using extracellular flux. *Drug Discov Today* 13:268-274.

Gottgens, B. 2015. Regulatory network control of blood stem cells. *Blood* 125:2614-2620.

Guitart, A.V., C. Subramani, A. Armesilla-Diaz, G. Smith, C. Sepulveda, D. Gezer, M. Vukovic, K. Dunn, P. Pollard, T.L. Holyoake, T. Enver, P.J. Ratcliffe, and K.R. Kranc. 2013. Hif-2alpha is not essential for cell-autonomous hematopoietic stem cell maintenance. *Blood* 122:1741-1745.

Hewitson, K.S., B.M. Lienard, M.A. McDonough, I.J. Clifton, D. Butler, A.S. Soares, N.J. Oldham, L.A. McNeill, and C.J. Schofield. 2007. Structural and mechanistic studies on the inhibition of the hypoxia-inducible transcription factor hydroxylases by tricarboxylic acid cycle intermediates. *J Biol Chem* 282:3293-3301.

Isaacs, J.S., Y.J. Jung, D.R. Mole, S. Lee, C. Torres-Cabala, Y.L. Chung, M. Merino, J. Trepel, B. Zbar, J. Toro, P.J. Ratcliffe, W.M. Linehan, and L. Neckers. 2005. HIF overexpression correlates with biallelic loss of fumarate hydratase in renal cancer: novel role of fumarate in regulation of HIF stability. *Cancer Cell* 8:143-153.

Jiao, B., C.F. Wu, Y. Liang, H.M. Chen, S.M. Xiong, B. Chen, J.Y. Shi, Y.Y. Wang, J.H. Wang, Y. Chen, J.M. Li, L.J. Gu, J.Y. Tang, Z.X. Shen, B.W. Gu, W.L. Zhao, Z. Chen, and S.J. Chen. 2009. AML1-ETO9a is correlated with C-KIT overexpression/mutations and indicates poor disease outcome in t(8;21) acute myeloid leukemia-M2. *Leukemia* 23:1598-1604.

Keuper, M., M. Jastroch, C.X. Yi, P. Fischer-Posovszky, M. Wabitsch, M.H. Tschop, and S.M. Hofmann. 2014. Spare mitochondrial respiratory capacity permits human adipocytes to maintain ATP homeostasis under hypoglycemic conditions. *FASEB J* 28:761-770.

Kranc, K.R., H. Schepers, N.P. Rodrigues, S. Bamforth, E. Villadsen, H. Ferry, T. Bouriez-Jones, M. Sigvardsson, S. Bhattacharya, S.E. Jacobsen, and T. Enver. 2009. Cited2 is an essential regulator of adult hematopoietic stem cells. *Cell Stem Cell* 5:659-665.

Krivtsov, A.V., and S.A. Armstrong. 2007. MLL translocations, histone modifications and leukaemia stem-cell development. *Nat Rev Cancer* 7:823-833.

Kroon, E., J. Krosl, U. Thorsteinsdottir, S. Baban, A.M. Buchberg, and G. Sauvageau. 1998. Hoxa9 transforms primary bone marrow cells through specific collaboration with Meis1a but not Pbx1b. *EMBO J* 17:3714-3725.

Kuhn, R., F. Schwenk, M. Aguet, and K. Rajewsky. 1995. Inducible gene targeting in mice. *Science* 269:1427-1429.

Lagadinou, E.D., A. Sach, K. Callahan, R.M. Rossi, S.J. Neering, M. Minhajuddin, J.M. Ashton, S. Pei, V. Grose, K.M. O'Dwyer, J.L. Liesveld, P.S. Brookes, M.W. Becker, and C.T. Jordan. 2013. BCL-2 inhibition targets oxidative phosphorylation and selectively eradicates quiescent human leukemia stem cells. *Cell Stem Cell* 12:329-341.

Launonen, V., O. Vierimaa, M. Kiuru, J. Isola, S. Roth, E. Pukkala, P. Sistonen, R. Herva, and L.A. Aaltonen. 2001. Inherited susceptibility to uterine leiomyomas and renal cell cancer. *Proc Natl Acad Sci U S A* 98:3387-3392.

Lavallee, V.P., I. Baccelli, J. Krosl, B. Wilhelm, F. Barabe, P. Gendron, G. Boucher, S. Lemieux, A. Marinier, S. Meloche, J. Hebert, and G. Sauvageau. 2015. The transcriptomic landscape and directed chemical interrogation of MLL-rearranged acute myeloid leukemias. *Nat Genet* 47:1030-1037.

Lawrence, H.J., S. Rozenfeld, C. Cruz, K. Matsukuma, A. Kwong, L. Komuves, A.M. Buchberg, and C. Largman. 1999. Frequent co-expression of the HOXA9 and MEIS1 homeobox genes in human myeloid leukemias. *Leukemia* 13:1993-1999.

Letouze, E., C. Martinelli, C. Loriot, N. Burnichon, N. Abermil, C. Ottolenghi, M. Janin, M. Menara, A.T. Nguyen, P. Benit, A. Buffet, C. Marcaillou, J. Bertherat, L. Amar, P. Rustin, A. De Reynies, A.P. Gimenez-Roqueplo, and J. Favier. 2013. SDH mutations establish a hypermethylator phenotype in paraganglioma. *Cancer Cell* 23:739-752.

Lopez-Pedrera, C., J.M. Villalba, E. Siendones, N. Barbarroja, C. Gomez-Diaz, A. Rodriguez-Ariza, P. Buendia, A. Torres, and F. Velasco. 2006. Proteomic analysis of acute myeloid leukemia: Identification of potential early biomarkers and therapeutic targets. *Proteomics* 6 Suppl 1:S293-299.

Manesia, J.K., Z. Xu, D. Broekaert, R. Boon, A. van Vliet, G. Eelen, T. Vanwelden, S. Stegen, N. Van Gastel, A. Pascual-Montano, S.M. Fendt, G. Carmeliet, P. Carmeliet, S. Khurana, and C.M. Verfaillie. 2015. Highly proliferative primitive fetal liver hematopoietic stem cells are fueled by oxidative metabolic pathways. *Stem Cell Res* 15:715-721.

Miharada, K., V. Sigurdsson, and S. Karlsson. 2014. Dppa5 improves hematopoietic stem cell activity by reducing endoplasmic reticulum stress. *Cell Rep* 7:1381-1392.

Mortensen, M., E.J. Soilleux, G. Djordjevic, R. Tripp, M. Lutteropp, E. Sadighi-Akha, A.J. Stranks, J. Glanville, S. Knight, S.-E. W. Jacobsen, K.R. Kranc, and A.K. Simon. 2011. The autophagy protein Atg7 is essential for hematopoietic stem cell maintenance. *The Journal of Experimental Medicine* 208:455-467.

O'Flaherty, L., J. Adam, L.C. Heather, A.V. Zhdanov, Y.L. Chung, M.X. Miranda, J. Croft, S. Olpin, K. Clarke, C.W. Pugh, J. Griffiths, D. Papkovsky, H. Ashrafian, P.J. Ratcliffe, and P.J. Pollard. 2010. Dysregulation of hypoxia pathways in fumarate hydratase-deficient cells is independent of defective mitochondrial metabolism. *Hum Mol Genet* 19:3844-3851.

Pollard, P.J., B. Spencer-Dene, D. Shukla, K. Howarth, E. Nye, M. El-Bahrawy, M. Deheragoda, M. Joannou, S. McDonald, A. Martin, P. Igarashi, S. Varsani-Brown, I. Rosewell, R. Poulsom, P. Maxwell, G.W. Stamp, and I.P. Tomlinson. 2007. Targeted inactivation of fh1

causes proliferative renal cyst development and activation of the hypoxia pathway. *Cancer Cell* 11:311-319.

Ryan, H.E., M. Poloni, W. McNulty, D. Elson, M. Gassmann, J.M. Arbeit, and R.S. Johnson. 2000. Hypoxia-inducible factor-1alpha is a positive factor in solid tumor growth. *Cancer Res* 60:4010-4015.

Sass, E., E. Blachinsky, S. Karniely, and O. Pines. 2001. Mitochondrial and cytosolic isoforms of yeast fumarase are derivatives of a single translation product and have identical amino termini. *J Biol Chem* 276:46111-46117.

Signer, R.A., J.A. Magee, A. Salic, and S.J. Morrison. 2014. Haematopoietic stem cells require a highly regulated protein synthesis rate. *Nature* 509:49-54.

Simsek, T., F. Kocabas, J. Zheng, R.J. Deberardinis, A.I. Mahmoud, E.N. Olson, J.W. Schneider, C.C. Zhang, and H.A. Sadek. 2010. The distinct metabolic profile of hematopoietic stem cells reflects their location in a hypoxic niche. *Cell Stem Cell* 7:380-390.

Singh, R.P., K. Franke, J. Kalucka, S. Mamlouk, A. Muschter, A. Gembarska, T. Grinenko, C. Willam, R. Naumann, K. Anastassiadis, A.F. Stewart, S. Bornstein, T. Chavakis, G. Breier, C. Waskow, and B. Wielockx. 2013. HIF prolyl hydroxylase 2 (PHD2) is a critical regulator of hematopoietic stem cell maintenance during steady-state and stress. *Blood* 121:5158-5166.

Smith, L.L., J. Yeung, B.B. Zeisig, N. Popov, I. Huijbers, J. Barnes, A.J. Wilson, E. Taskesen, R. Delwel, J. Gil, M. Van Lohuizen, and C.W. So. 2011. Functional Crosstalk between Bmi1 and MLL/Hoxa9 Axis in Establishment of Normal Hematopoietic and Leukemic Stem Cells. *Cell Stem Cell* 8:649-662.

Somervaille, T.C., and M.L. Cleary. 2006. Identification and characterization of leukemia stem cells in murine MLL-AF9 acute myeloid leukemia. *Cancer Cell* 10:257-268.

Stein, I., Y. Peleg, S. Even-Ram, and O. Pines. 1994. The single translation product of the FUM1 gene (fumarase) is processed in mitochondria before being distributed between the cytosol and mitochondria in Saccharomyces cerevisiae. *Mol Cell Biol* 14:4770-4778.

Stewart, M.H., M. Albert, P. Sroczynska, V.A. Cruickshank, Y. Guo, D.J. Rossi, K. Helin, and T. Enver. 2015. The histone demethylase Jarid1b is required for hematopoietic stem cell self-renewal in mice. *Blood* 125:2075-2078.

Subramanian, A., P. Tamayo, V.K. Mootha, S. Mukherjee, B.L. Ebert, M.A. Gillette, A. Paulovich, S.L. Pomeroy, T.R. Golub, E.S. Lander, and J.P. Mesirov. 2005. Gene set enrichment analysis: a knowledge-based approach for interpreting genome-wide expression profiles. *Proc Natl Acad Sci U S A* 102:15545-15550.

Suda, T., K. Takubo, and G.L. Semenza. 2011. Metabolic regulation of hematopoietic stem cells in the hypoxic niche. *Cell Stem Cell* 9:298-310.

Sullivan, L.B., E. Martinez-Garcia, H. Nguyen, A.R. Mullen, E. Dufour, S. Sudarshan, J.D. Licht, R.J. Deberardinis, and N.S. Chandel. 2013. The proto-oncometabolite fumarate binds glutathione to amplify ROS-dependent signaling. *Mol Cell* 51:236-248.

Takubo, K., N. Goda, W. Yamada, H. Iriuchishima, E. Ikeda, Y. Kubota, H. Shima, R.S. Johnson, A. Hirao, M. Suematsu, and T. Suda. 2010. Regulation of the HIF-1alpha level is essential for hematopoietic stem cells. *Cell Stem Cell* 7:391-402.

Takubo, K., G. Nagamatsu, C.I. Kobayashi, A. Nakamura-Ishizu, H. Kobayashi, E. Ikeda, N. Goda, Y. Rahimi, R.S. Johnson, T. Soga, A. Hirao, M. Suematsu, and T. Suda. 2013. Regulation of glycolysis by Pdk functions as a metabolic checkpoint for cell cycle quiescence in hematopoietic stem cells. *Cell Stem Cell* 12:49-61.

Tanaka, K.R., and W.N. Valentine. 1961. Fumarase activity of human leukocytes and erythrocytes. *Blood* 17:328-333.

Ternette, N., M. Yang, M. Laroyia, M. Kitagawa, L. O'Flaherty, K. Wolhulter, K. Igarashi, K. Saito, K. Kato, R. Fischer, A. Berquand, B.M. Kessler, T. Lappin, N. Frizzell, T. Soga, J. Adam, and P.J. Pollard. 2013. Inhibition of mitochondrial aconitase by succination in fumarate hydratase deficiency. *Cell Rep* 3:689-700.

Tomlinson, I.P., N.A. Alam, A.J. Rowan, E. Barclay, E.E. Jaeger, D. Kelsell, I. Leigh, P. Gorman, H. Lamlum, S. Rahman, R.R. Roylance, S. Olpin, S. Bevan, K. Barker, N. Hearle, R.S. Houlston, M. Kiuru, R. Lehtonen, A. Karhu, S. Vilkki, P. Laiho, C. Eklund, O. Vierimaa, K. Aittomaki, M. Hietala, P. Sistonen, A. Paetau, R. Salovaara, R. Herva, V. Launonen, L.A. Aaltonen, and C. Multiple Leiomyoma. 2002. Germline mutations in FH predispose to dominantly inherited uterine fibroids, skin leiomyomata and papillary renal cell cancer. *Nat Genet* 30:406-410.

Tregoning, S., W. Salter, D.R. Thorburn, M. Durkie, M. Panayi, J.Y. Wu, A. Easterbrook, and D.J. Coman. 2013. Fumarase deficiency in dichorionic diamniotic twins. *Twin Res Hum Genet* 16:1117-1120.

van der Windt, G.J., B. Everts, C.H. Chang, J.D. Curtis, T.C. Freitas, E. Amiel, E.J. Pearce, and E.L. Pearce. 2012. Mitochondrial respiratory capacity is a critical regulator of CD8+ T cell memory development. *Immunity* 36:68-78.

van Galen, P., A. Kreso, N. Mbong, D.G. Kent, T. Fitzmaurice, J.E. Chambers, S. Xie, E. Laurenti, K. Hermans, K. Eppert, S.J. Marciniak, J.C. Goodall, A.R. Green, B.G. Wouters, E. Wienholds, and J.E. Dick. 2014. The unfolded protein response governs integrity of the haematopoietic stem-cell pool during stress. *Nature* 510:268-272.

Velasco-Hernandez, T., A. Hyrenius-Wittsten, M. Rehn, D. Bryder, and J. Cammenga. 2014. HIF-1alpha can act as a tumor suppressor gene in murine Acute Myeloid Leukemia. *Blood*

Vukovic, M., A.V. Guitart, C. Sepulveda, A. Villacreces, E. O'Duibhir, T.I. Panagopoulou, A. Ivens, J. Menendez-Gonzalez, J.M. Iglesias, L. Allen, F. Glykofrydis, C. Subramani, A. Armesilla-Diaz, A.E. Post, K. Schaak, D. Gezer, C.W. So, T.L. Holyoake, A. Wood, D. O'Carroll, P.J. Ratcliffe, and K.R. Kranc. 2015. Hif-1alpha and Hif-2alpha synergize to suppress AML development but are dispensable for disease maintenance. *J Exp Med*

Vukovic, M., C. Sepulveda, C. Subramani, A.V. Guitart, J. Mohr, L. Allen, T.I. Panagopoulou, J. Paris, H. Lawson, A. Villacreces, A. Armesilla-Diaz, D. Gezer, T.L. Holyoake, P.J. Ratcliffe, and K.R. Kranc. 2016. Adult haematopoietic stem cells lacking Hif-1alpha self-renew normally. *Blood*

Wang, Y., A.V. Krivtsov, A.U. Sinha, T.E. North, W. Goessling, Z. Feng, L.I. Zon, and S.A. Armstrong. 2010. The Wnt/beta-catenin pathway is required for the development of leukemia stem cells in AML. *Science* 327:1650-1653.

Wang, Y.H., W.J. Israelsen, D. Lee, V.W. Yu, N.T. Jeanson, C.B. Clish, L.C. Cantley, M.G. Vander Heiden, and D.T. Scadden. 2014. Cell-state-specific metabolic dependency in hematopoiesis and leukemogenesis. *Cell* 158:1309-1323.

Weissman, I.L., and J.A. Shizuru. 2008. The origins of the identification and isolation of hematopoietic stem cells, and their capability to induce donor-specific transplantation tolerance and treat autoimmune diseases. *Blood* 112:3543-3553.

Xiao, M., H. Yang, W. Xu, S. Ma, H. Lin, H. Zhu, L. Liu, Y. Liu, C. Yang, Y. Xu, S. Zhao, D. Ye, Y. Xiong, and K.L. Guan. 2012. Inhibition of alpha-KG-dependent histone and DNA demethylases by fumarate and succinate that are accumulated in mutations of FH and SDH tumor suppressors. *Genes Dev* 26:1326-1338.

Yadava, N., and D.G. Nicholls. 2007. Spare respiratory capacity rather than oxidative stress regulates glutamate excitotoxicity after partial respiratory inhibition of mitochondrial complex I with rotenone. *J Neurosci* 27:7310-7317.

Yang, M., T. Soga, and P.J. Pollard. 2013. Oncometabolites: linking altered metabolism with cancer. *J Clin Invest* 123:3652-3658.

Yeung, J., M.T. Esposito, A. Gandillet, B.B. Zeisig, E. Griessinger, D. Bonnet, and C.W. So. 2010. beta-Catenin mediates the establishment and drug resistance of MLL leukemic stem cells. *Cancer Cell* 18:606-618.

Yu, W.M., X. Liu, J. Shen, O. Jovanovic, E.E. Pohl, S.L. Gerson, T. Finkel, H.E. Broxmeyer, and C.K. Qu. 2013. Metabolic regulation by the mitochondrial phosphatase PTPMT1 is required for hematopoietic stem cell differentiation. *Cell Stem Cell* 12:62-74.

Zheng, L., S. Cardaci, L. Jerby, E.D. MacKenzie, M. Sciacovelli, T.I. Johnson, E. Gaude, A. King, J.D. Leach, R. Edrada-Ebel, A. Hedley, N.A. Morrice, G. Kalna, K. Blyth, E. Ruppin, C. Frezza, and E. Gottlieb. 2015. Fumarate induces redox-dependent senescence by modifying glutathione metabolism. *Nat Commun* 6:6001.

Zheng, L., E.D. Mackenzie, S.A. Karim, A. Hedley, K. Blyth, G. Kalna, D.G. Watson, P. Szlosarek, C. Frezza, and E. Gottlieb. 2013. Reversed argininosuccinate lyase activity in fumarate hydratase-deficient cancer cells. *Cancer Metab* 1:12.

Zuber, J., I. Radtke, T.S. Pardee, Z. Zhao, A.R. Rappaport, W. Luo, M.E. McCurrach, M.M. Yang, M.E. Dolan, S.C. Kogan, J.R. Downing, and S.W. Lowe. 2009. Mouse models of human AML accurately predict chemotherapy response. *Genes Dev* 23:877-889.

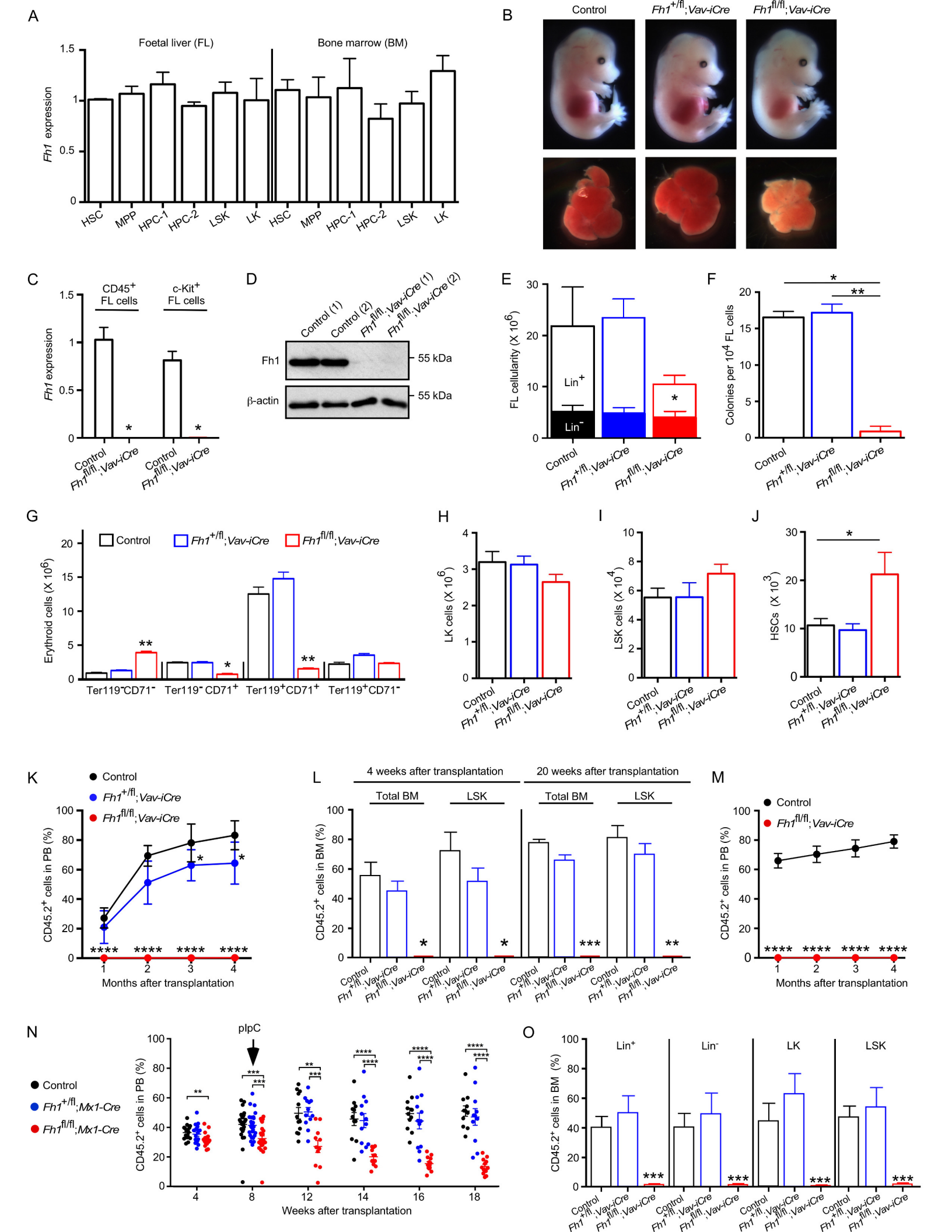
A
Foetal liver (FL)
Bone marrow (BM)
Fh1 expression
HSC
MPP
HPC-1
HPC-2
LSK
LK
B
Control
Fh1+/fl;Vav-iCre
Fh1fl/fl;Vav-iCre
C
CD45+ FL cells
c-Kit+ FL cells
D
Control (1)
Control (2)
Fh1fl/fl;Vav-iCre (1)
Fh1fl/fl;Vav-iCre (2)
Fh1
β-actin
55 kDa
E
FL cellularity (X 10^6)
Lin+
Lin-
F
Colonies per 10^4 FL cells
G
Erythroid cells (X 10^6)
Ter119-CD71-
Ter119-CD71+
Ter119+CD71+
Ter119+CD71-
H
LK cells (X 10^6)
I
LSK cells (X 10^4)
J
HSCs (X 10^3)
K
CD45.2+ cells in PB (%)
Months after transplantation
L
4 weeks after transplantation
20 weeks after transplantation
Total BM
LSK
CD45.2+ cells in BM (%)
M
N
pIpC
Fh1+/fl;Mx1-Cre
Fh1fl/fl;Mx1-Cre
Weeks after transplantation
O
Lin+
Lin-
LK
LSK

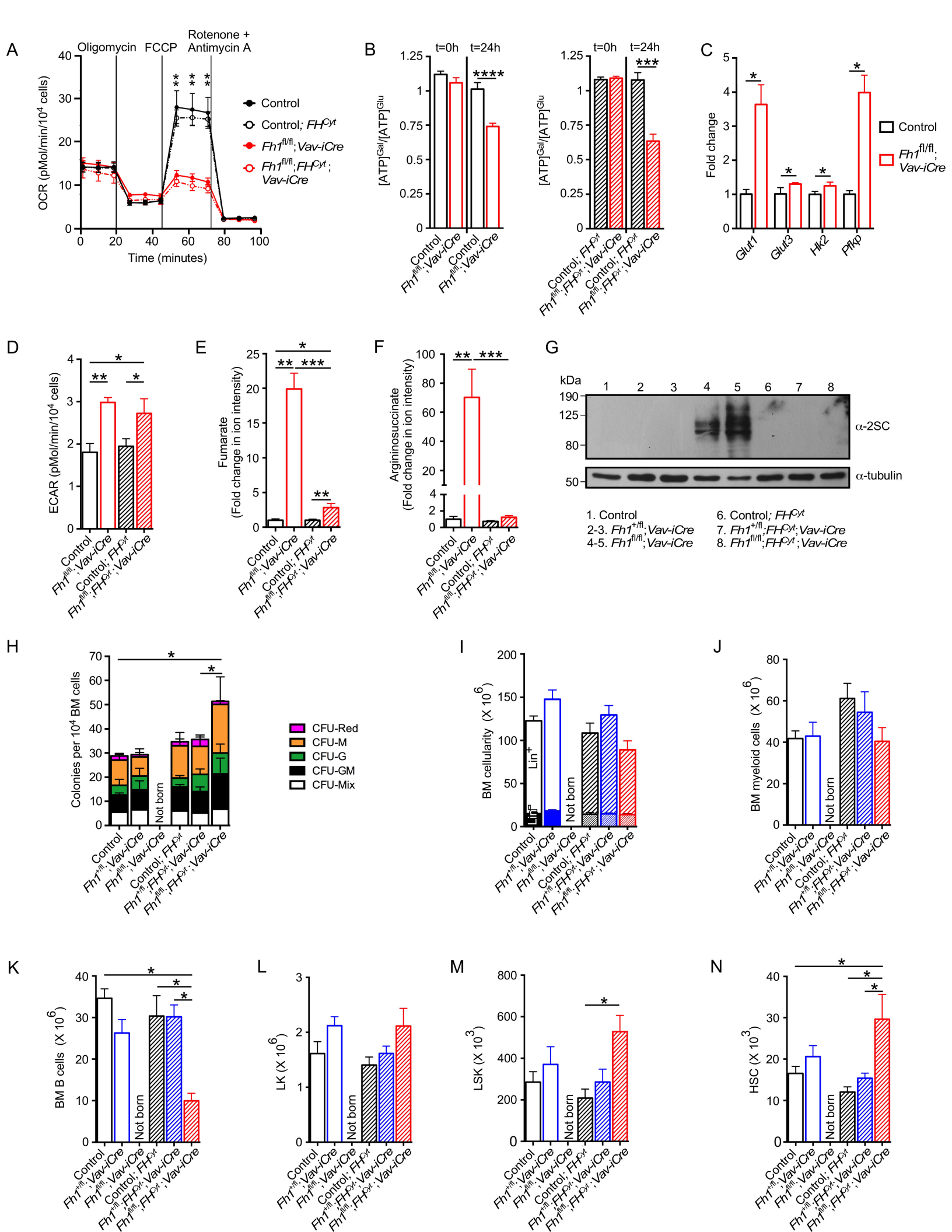
A
Oligomycin
FCCP
Rotenone + Antimycin A
OCR (pMol/min/10^4 cells)
Time (minutes)
Control
Control; FH^Cyt
Fh1^fl/fl;Vav-iCre
Fh1^fl/fl;FH^Cyt; Vav-iCre
B
t=0h
t=24h
[ATP]^Gal/[ATP]^Glu
****
***
Control
Fh1^fl/fl;Vav-iCre
Control; FH^Cyt
Fh1^fl/fl;FH^Cyt;Vav-iCre
C
Fold change
Glut1
Glut3
Hk2
Pfkp
Control
Fh1^fl/fl; Vav-iCre
D
ECAR (pMol/min/10^4 cells)
E
Fumarate (Fold change in ion intensity)
F
Argininosuccinate (Fold change in ion intensity)
G
kDa
1 2 3 4 5 6 7 8
190
125
80
50
α-2SC
α-tubulin
1. Control
2-3. Fh1^+/fl;Vav-iCre
4-5. Fh1^fl/fl;Vav-iCre
6. Control; FH^Cyt
7. Fh1^+/fl;FH^Cyt;Vav-iCre
8. Fh1^fl/fl;FH^Cyt;Vav-iCre
H
Colonies per 10^4 BM cells
CFU-Red
CFU-M
CFU-G
CFU-GM
CFU-Mix
Not born
I
BM cellularity (X 10^6)
Lin+
Lin-
J
BM myeloid cells (X 10^6)
K
BM B cells (X 10^6)
L
LK (X 10^6)
M
LSK (X 10^3)
N
HSC (X 10^3)

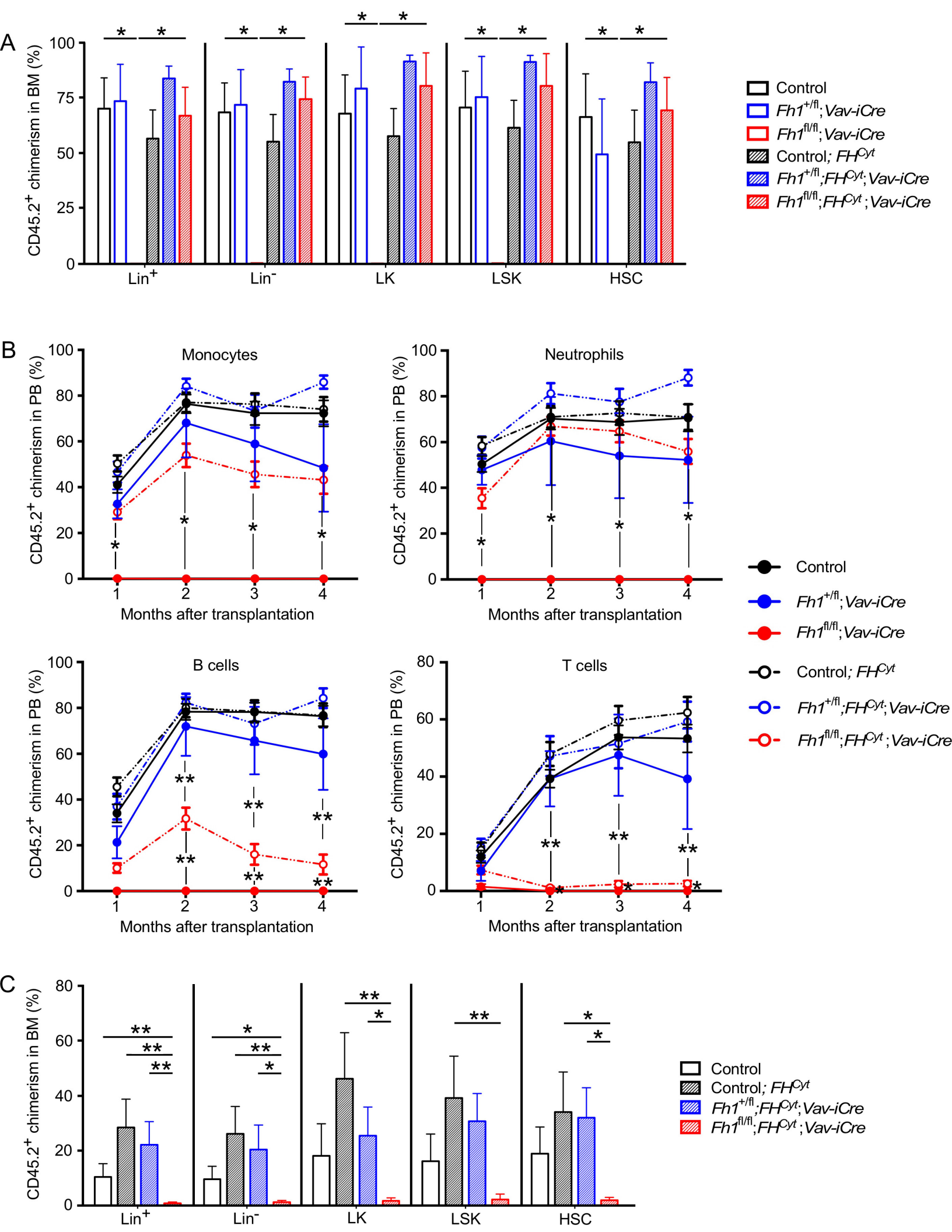
A
CD45.2+ chimerism in BM (%)
Lin+
Lin-
LK
LSK
HSC
Control
Fh1+/fl;Vav-iCre
Fh1fl/fl;Vav-iCre
Control; FHCyt
Fh1+/fl;FHCyt;Vav-iCre
Fh1fl/fl;FHCyt;Vav-iCre
B
Monocytes
Neutrophils
B cells
T cells
CD45.2+ chimerism in PB (%)
Months after transplantation
C
CD45.2+ chimerism in BM (%)
Lin+
Lin-
LK
LSK
HSC

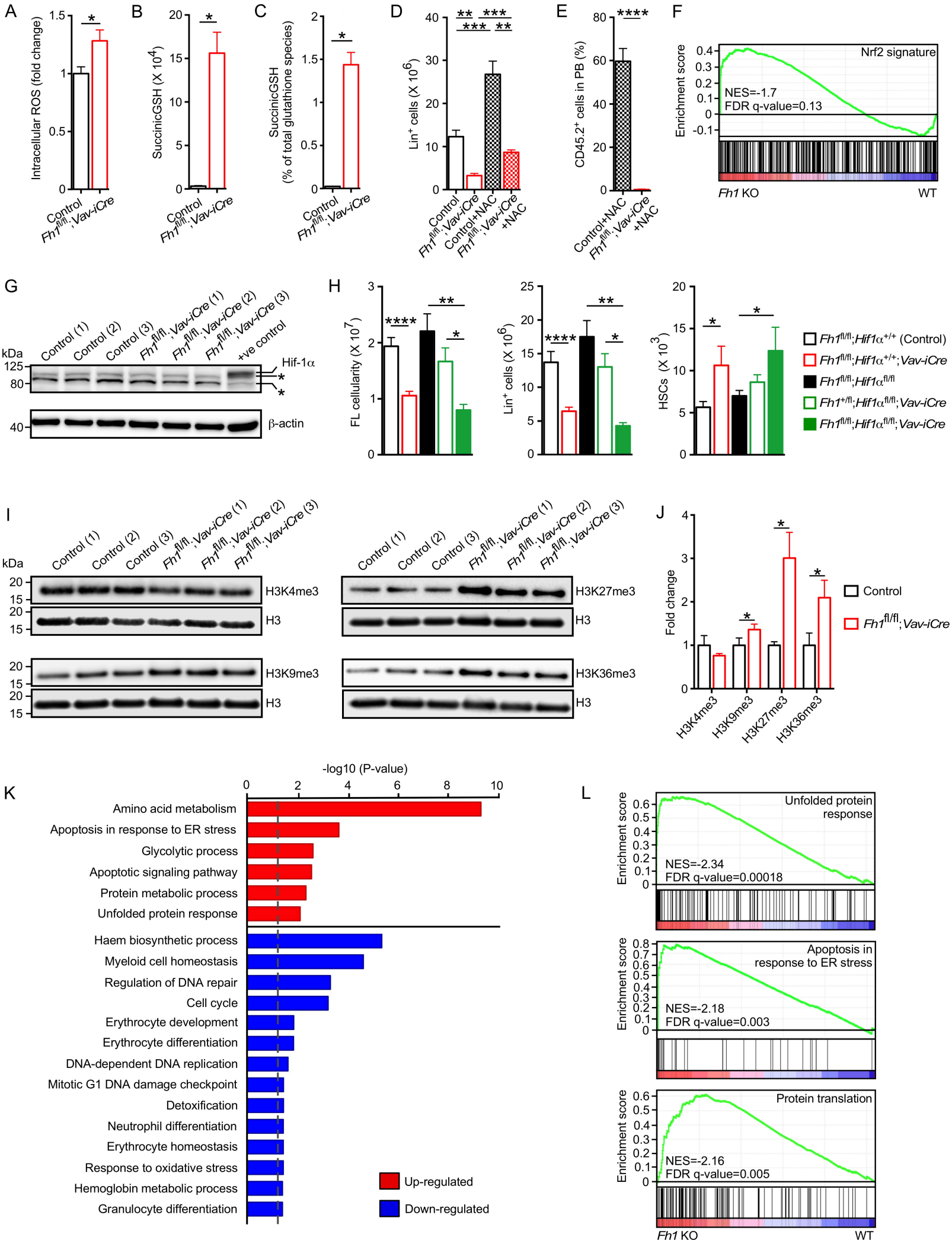
A
Intracellular ROS (fold change)
Control
Fh1fl/fl;Vav-iCre
B
SuccinicGSH (X 10^4)
C
SuccinicGSH (% of total glutathione species)
D
Lin+ cells (X 10^6)
Control+NAC
Fh1fl/fl;Vav-iCre +NAC
E
CD45.2+ cells in PB (%)
F
Nrf2 signature
NES=-1.7
FDR q-value=0.13
Enrichment score
Fh1 KO
WT
G
kDa
Control (1)
Control (2)
Control (3)
Fh1fl/fl;Vav-iCre (1)
Fh1fl/fl;Vav-iCre (2)
Fh1fl/fl;Vav-iCre (3)
+ve control
Hif-1α
β-actin
H
FL cellularity (X 10^7)
Lin+ cells (X 10^6)
HSCs (X 10^3)
Fh1fl/fl;Hif1α+/+ (Control)
Fh1fl/fl;Hif1α+/+;Vav-iCre
Fh1fl/fl;Hif1αfl/fl
Fh1+/fl;Hif1αfl/fl;Vav-iCre
Fh1fl/fl;Hif1αfl/fl;Vav-iCre
I
H3K4me3
H3K27me3
H3K9me3
H3K36me3
H3
J
Fold change
Control
Fh1fl/fl;Vav-iCre
K
-log10 (P-value)
Amino acid metabolism
Apoptosis in response to ER stress
Glycolytic process
Apoptotic signaling pathway
Protein metabolic process
Unfolded protein response
Haem biosynthetic process
Myeloid cell homeostasis
Regulation of DNA repair
Cell cycle
Erythrocyte development
Erythrocyte differentiation
DNA-dependent DNA replication
Mitotic G1 DNA damage checkpoint
Detoxification
Neutrophil differentiation
Erythrocyte homeostasis
Response to oxidative stress
Hemoglobin metabolic process
Granulocyte differentiation
Up-regulated
Down-regulated
L
Unfolded protein response
NES=-2.34
FDR q-value=0.00018
Apoptosis in response to ER stress
NES=-2.18
FDR q-value=0.003
Protein translation
NES=-2.16
FDR q-value=0.005
Enrichment score
Fh1 KO
WT

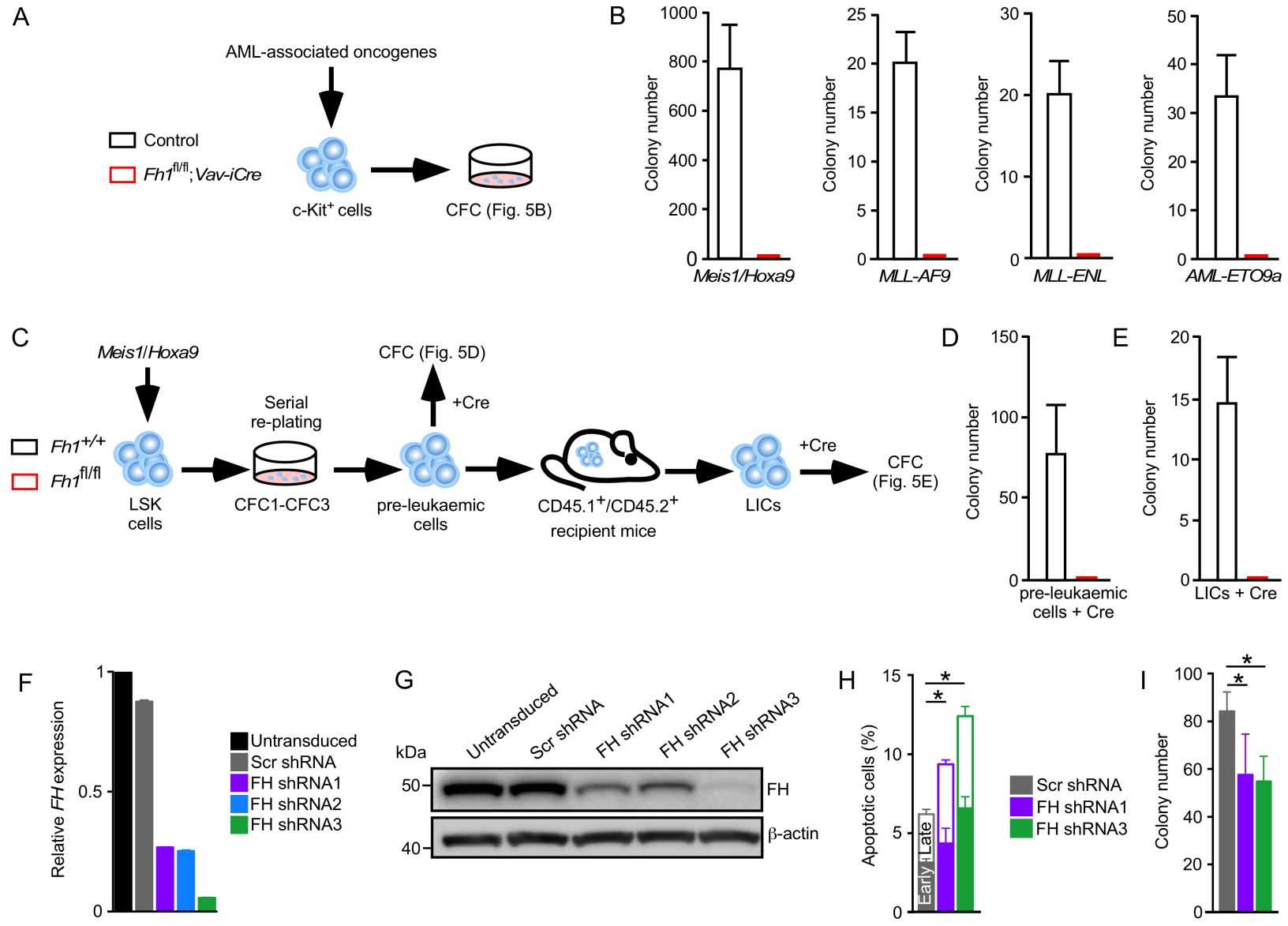
A
AML-associated oncogenes
Control
Fh1fl/fl;Vav-iCre
c-Kit+ cells
CFC (Fig. 5B)
B
Colony number
Meis1/Hoxa9
MLL-AF9
MLL-ENL
AML-ETO9a
C
Meis1/Hoxa9
Fh1+/+
Fh1fl/fl
LSK cells
Serial re-plating
CFC1-CFC3
CFC (Fig. 5D)
+Cre
pre-leukaemic cells
CD45.1+/CD45.2+ recipient mice
LICs
+Cre
CFC (Fig. 5E)
D
Colony number
pre-leukaemic cells + Cre
E
Colony number
LICs + Cre
F
Relative FH expression
Untransduced
Scr shRNA
FH shRNA1
FH shRNA2
FH shRNA3
G
kDa
Untransduced
Scr shRNA
FH shRNA1
FH shRNA2
FH shRNA3
FH
β-actin
H
Apoptotic cells (%)
Early+Late
Scr shRNA
FH shRNA1
FH shRNA3
I
Colony number

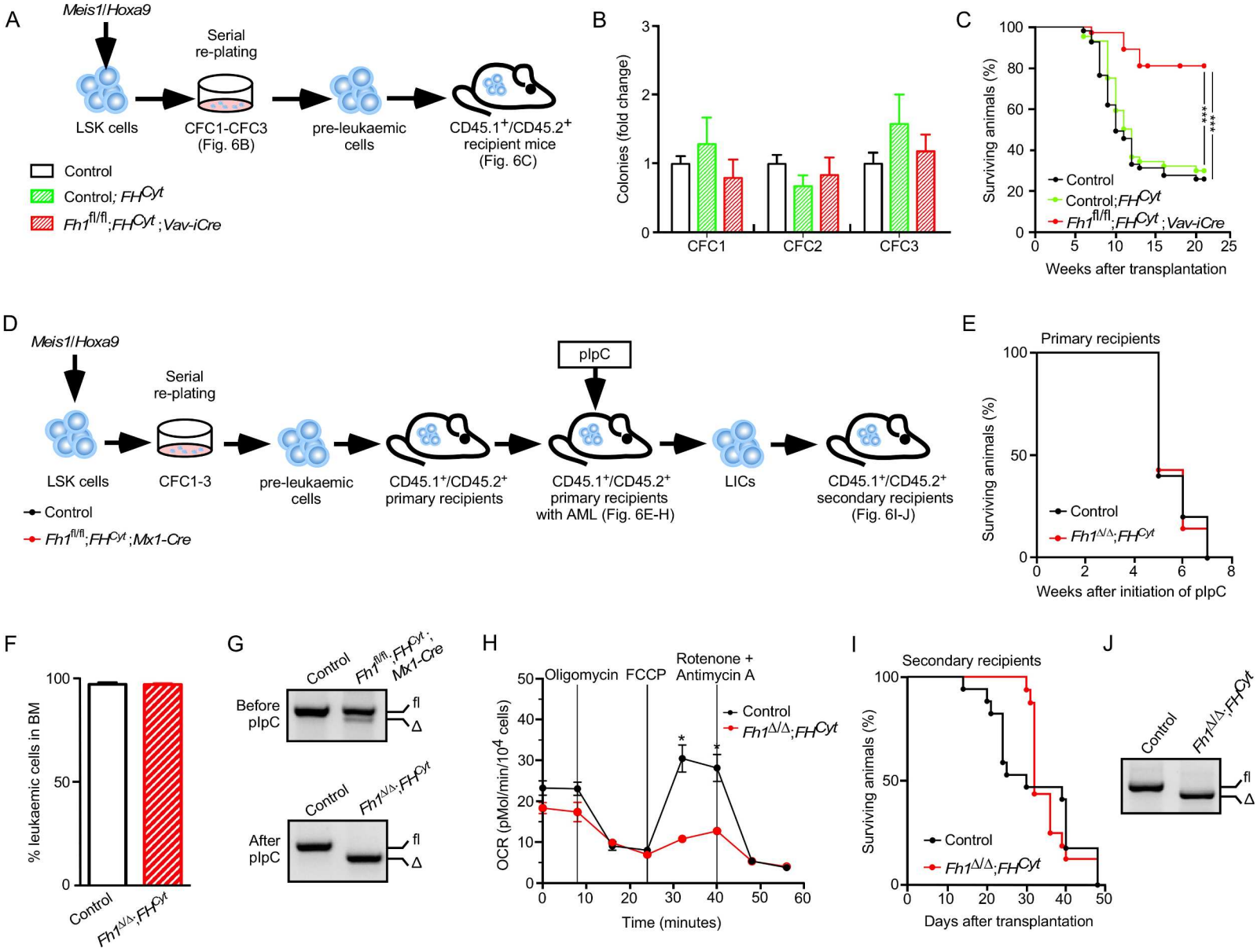
A
Meis1/Hoxa9
Serial re-plating
LSK cells
CFC1-CFC3 (Fig. 6B)
pre-leukaemic cells
CD45.1+/CD45.2+ recipient mice (Fig. 6C)
Control
Control; FHCyt
Fh1fl/fl;FHCyt;Vav-iCre
B
Colonies (fold change)
CFC1
CFC2
CFC3
C
Surviving animals (%)
Weeks after transplantation
***
***
Control
Control;FHCyt
Fh1fl/fl;FHCyt;Vav-iCre
D
Meis1/Hoxa9
Serial re-plating
pIpC
LSK cells
CFC1-3
pre-leukaemic cells
CD45.1+/CD45.2+ primary recipients
CD45.1+/CD45.2+ primary recipients with AML (Fig. 6E-H)
LICs
CD45.1+/CD45.2+ secondary recipients (Fig. 6I-J)
Control
Fh1fl/fl;FHCyt;Mx1-Cre
E
Primary recipients
Surviving animals (%)
Weeks after initiation of pIpC
Control
Fh1Δ/Δ;FHCyt
F
% leukaemic cells in BM
Control
Fh1Δ/Δ;FHCyt
G
Control
Fh1fl/fl;FHCyt;Mx1-Cre
Before pIpC
fl
Δ
Control
Fh1Δ/Δ;FHCyt
After pIpC
fl
Δ
H
Oligomycin
FCCP
Rotenone + Antimycin A
OCR (pMol/min/10^4 cells)
Time (minutes)
Control
Fh1Δ/Δ;FHCyt
I
Secondary recipients
Surviving animals (%)
Days after transplantation
Control
Fh1Δ/Δ;FHCyt
J
Control
Fh1Δ/Δ;FHCyt
fl
Δ